Energy & Buildings 202 (2019) 109334

Contents lists available at ScienceDirect

Energy & Buildings

journal homepage: www.elsevier.com/locate/enbuild

Conditioning using ceramic floor panels with capillary tube mats and solar thermal panels on the Mediterranean coast: Energy savings and investment amortisation

Víctor Echarri-Iribarren

Departamento de Construcciones Arquitectónicas, Universidad de Alicante, Carretera de San Vicente s/n, 03690 San Vicente, Alicante, Spain

ARTICLE INFO

Article history:
Received 13 April 2019
Revised 19 June 2019
Accepted 24 July 2019
Available online 25 July 2019

Keywords:
Thermal ceramic panel
Capillary tube systems
Solar thermal panels
Energy saving
Renewable energy
Solar refrigeration technology

ABSTRACT

Radiant floor conditioning installations that distribute water through PPR capillary tube mats bring about significant energy savings and high standards of comfort. Their design usually includes air-water heat pumps and fan-coil dehumidification. They also allow incorporating solar thermal panel energy. In summer mode, they can also be combined with absorption systems with lithium bromide, or solar cold based on lithium chloride. In this way, annual energy demand is further reduced by low water channel transport and reduced heat flows through the enclosures. This study focused on the application of large-format radiant floor thermal ceramic panels (TCP), with capillary tube mats, in the Museum of the University of Alicante (MUA). The water distribution system was made of two heat pumps combined with a solar thermal panel rooftop installation. Using thermal simulation tools, the MUA's annual energy demand was quantified over various scenarios. An energy saving of 24.91% was obtained compared to conventional all-air systems, and a 60.79% saving was obtained with the use of solar panels. User comfort levels and the energy consumptions of the various elements of the installation were also comparatively quantified. To finish, we calculated the investment amortisation periods for the TCP panels and solar panels.

1. Introduction

Recently designed or modernised buildings largely prefer radiant heating and cooling systems due to their energy efficiency and low exergy destruction [1]. The difference between radiant heating systems and conventional HVAC systems is that radiant heating systems heat surfaces rather than air, saving substantial amounts of energy while providing greater levels of comfort [2]. Much research in recent years has centred on quantifying hygrothermic comfort improvements and radiant system energy savings. He et al. quantified the thermal comfort of a group of 20 people by means of a radiant cooling desk, demonstrating the system's suitability and achieving notable emission powers [3]. Mustakallio et al. compared chilled beam, chilled beam combined with radiant panels and chilled ceiling with mixing ventilation systems, quantifying the improvements obtained from radiant systems [4]. Zhao et al. concluded that the cooling capacity of radiant floor cooling increases with high-intensity solar radiation and high-temperature envelope surfaces in large space buildings [5]. Zhou and He highlighted in their research the suitability of capillary network systems versus thick tube systems to distribute hot water [6].

1.1. Radiant surface conditioning systems based on capillary mats

The 1980s saw the development of hygrothermal radiant surface conditioning systems based on capillary mats of polypropylene tubes of about 3 mm in diameter, separated by approximately 10 mm from one another [7]. Cold or hot water circulates through these mats, providing conditioning in summer —with the help of a fan-coil dehumidification system— and winter. These systems can be applied to any interior walls —floors, wall, ceilings— by means of various techniques including plasterboard, false ceilings, false walls or plaster projection. They succeed in providing healthy, silent and comfortable air conditioning. These PPR capillary tube systems work mainly by radiation, and secondarily by convection. By moderately cooling or heating some walls, and conducting minimal dehumidification in summer, with no cold or hot air supply, notable advantages can be achieved compared to convective systems [8]. Sound levels drop considerably, the air moves at very low convection speeds, thus providing high comfort levels [9]; the air

E-mail address: victor.echarri@ua.es

https://doi.org/10.1016/j.enbuild.2019.109334

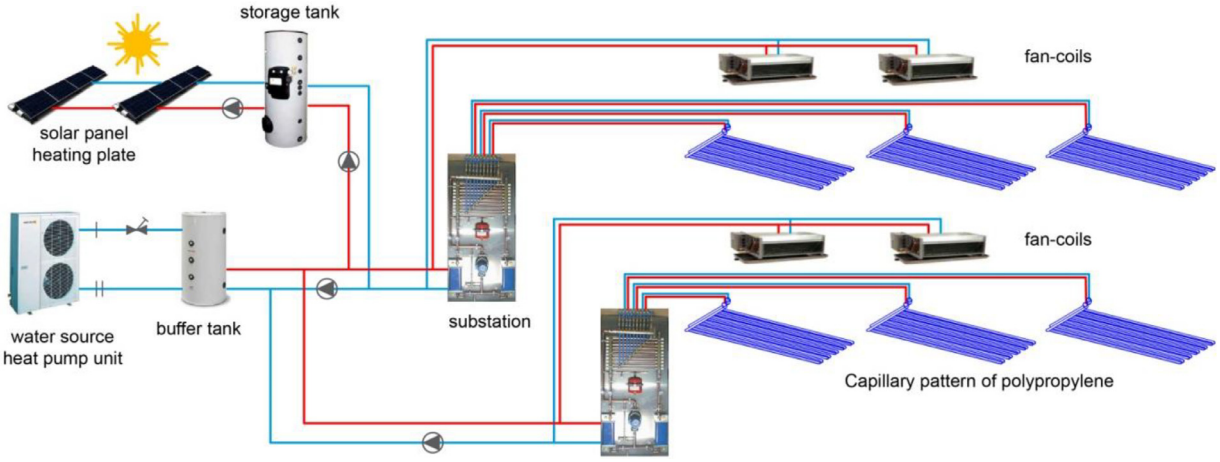

Fig. 1. Schematic diagram of a capillary mat installation, with fan-coils for dehumidification, and control substations.

temperature in summer is approximately 2–3 °C higher, and 2 °C lower in winter compared to convective systems. This way, comfort levels increase significantly. Furthermore, these radiant surface conditioning systems lead to substantial energy savings with respect to conventional air conditioning systems [10], as certified by reputable research institutes. The major factors include: water's greater capacity to transport energy compared to that of air; the system's self-regulation; and the reduction of thermal loads by heat transmission through the enclosures, as the indoor air is warmer in summer and cooler in winter.

Recent publications [11] have included schematic diagrams that describe how these capillary mat systems are implemented, including the use of alternative energies in the system (Fig. 1). When working with water at moderate temperatures in both summer and winter, it is feasible to use alternative energies: solar panels, chemical energy accumulation systems based on lithium chloride LiCl [12,13], absorption systems, geothermal energy systems [14], or seawater usage [15,16].

Radiant system solutions by means of hot or cold water distribution have often been implemented using prefabricated panels with a variety of finishing materials. Imanari et al. applied a radiant ceiling panel in office buildings, achieving remarkable results in terms of thermal comfort and energy savings, with a return on investment between 1 and 17 years, depending on the panel cost [17]. Miriel et al. proposed another radiant ceiling panel based on copper pipes with rigid aluminium diffusion fins, achieving a 10% reduction in energy consumption compared to the convective system [18]. In the same line, Zhang et al. worked with inclined aluminium fins, improving the cooling capacity of the suspended metal ceiling radiant panel by 19% [19]. Koca et al. studied the application of radiant wall heating panels and compared their efficiency with floor systems, concluding that heat transfer coefficients were 20% lower [20]. Other authors analysed the impact of finishing materials on radiant panels, such as Shin et al., who studied linoleum and oak wood [21]. Radiant panels have also been designed for floors, walls or ceilings that incorporate other water elements. Chae and Strand used a concentrate tube heat exchanger with two fluids, water and air, with promising results [22]; Ning et al. experimented with panels containing a thin layer of air, obtaining high efficiency when applying cooler water and thicker insulation in the water distribution pipes [23]; Lv et al. have recently experimented with radiant panels that can be filled with different liquids, such as Glycerol, obtaining greater efficiency than in the case of metal panels by means of a system in which different thermal conductivities depend on the distance to each panel's origin of distribution [24].

In recent years, ceramic materials have undergone remarkable technical improvements related to: mechanical resistance, behaviour towards external agents of humidity, temperature, or UV radiation, and almost non-existent water absorption. Added to the inalterability of porcelain stoneware, large-format and low thickness panels are now being produced, making them very light and easy to assemble. However, despite these wonderful qualities, porcelain stoneware applied to interior walls in buildings leads to thermal sensations that are less comfortable for users than other coating and finishing materials. High effusivity and thermal conductivity values compared to wood, linoleum or plaster, translates into the coatings stealing more energy from the user when in contact: they are considered cold and uncomfortable materials, especially in winter and in adverse weather conditions.

Taking into account the difficulty to synthesise new ceramic materials with better thermal performance, multilayer proposals have recently been put forward to produce more comfortable ceramic materials. They could thus compete with natural wood, high density wood, linoleum, etc. Radiant floor solutions using copper wire mesh, and Joule heating have been patented [25]. User comfort is improved, but this improvement comes at the expense of excessive energy use and costs, and greater CO_2 emissions. In addition, conditioning is possible only in winter, not in summer.

In this study, we applied large-format thermal ceramic panels (TCP) to the flooring of the Museum of the University of Alicante (MUA), in view of implementing radiant floor conditioning. Previous studies have applied TCP panels to walls or ceilings [26], but not to floors. The recent production of large-format, 20 mm thick ceramic pieces make it possible to apply them to flooring combined with PPR capillary mats. The MUA could be conditioned offering high levels of hygrothermal comfort quality in winter and summer with a fan-coil-based dehumidification system. The option of incorporating a rooftop thermal solar panel system was also examined. In this way, solar energy would be used in winter in the hot water production system, and used in summer to cool water by chemical energy (solar cold), providing alternative energy to the system. As we will see, notable energy savings would be achieved, with reasonable investment amortisation periods.

The MUA location is under a Mediterranean climate. It guarantees high levels of solar radiation on most summer and winter days. According to the Köpen-Geiger classification [27], it is classified as BSh: a warm semi-arid climate with hot or very hot summers and mild winters with very little rainfall [28]. The average annual temperature is 18.1 °C, the coldest month being January with 10.3 °C and the hottest month being August with an average

Table 1
Thermal parameters of possible finishing materials with KaRo capillary mats.

Material	Density kg/m^3	Specific Heat J/(Kg K)	Conductivity W/m K	Effusivity (W s$^{1/2}$)/(cm^2 K)
Steel	7850	460	47–58	1.30–1.45
Aluminium	2700	909	209–232	2.26–2.39
Ceramic Stoneware	2300	836	0.8–1.3	0.124–0.158
Ceramic Stoneware Flooring	2350	921	0.81	0.1324
Linoleum	5,35	1400	0.081	0.055
Beech Wood	800	1340	0.143	0.0392
Oak Wood	850	2386	0.209	0.0651
Glass	2700	833	0.81	0.1350
Plaster	1800	837	0.81	0.1104
Marble	2400	879	2.09	0.2099

Fig. 2. Application of TCP thermal ceramic panels in an office of the University of Alicante.

of 26.3 °C. According to the Spanish regulations in force at the time of building the CTE house (2013 modification) [29], it is located in a B3 climatic zone with an altitude of 240 m above sea level, letter B in winter and 3 in summer, according to the CTE-DB-HE table B1 classification (Climate Zones).

1.2. Large-format TCP ceramic panels

At present, the finishing materials most commonly used for capillary mats are plastering, plasterboards, false ceiling metal sheets, plaster projected onto walls or ceilings, reinforced concrete and other usual paving materials such as porcelain stoneware. Paving solutions with smoothed concrete and embedded mats have also been developed, with excellent outcomes. They have not been applied to porcelain stoneware on walls or ceilings due to technical execution problems, excessive weight and maintenance difficulties. However, new large-format porcelain stoneware pieces have been substantially improved technically over the last ten years allowing to produce prefabricated thermal ceramic panels with embedded mats [30].

The research group of the University of Alicante "Technology and Sustainability in Architecture" developed and patented in 2010 a Thermal Ceramic conditioning Panel (TCP) together with ASCER and the ITC [31]. The panel consists of one or two pieces of large-format and low-thickness porcelain stoneware [32] armoured with fiberglass on one of its faces, a capillary mat of polypropylene PPR tubes of 3.5 mm in diameter, separated every 10 mm, and conductive paste to adhere the capillary tube mat (Fig. 2). The initial dimensions were 300 cm x 100 cm x 3 mm, although larger panels measuring 320 cm x 160 cm x 9 mm are currently being manufactured. The solution is ideal for modular ceramic ceilings, wall plasterboards and ceiling-mounted large-format pieces, or even for baffle-type solutions, in which the panels are vertically suspended from the ceiling. When working with 3 mm pieces, 3 + 3 mm with fiberglass and polyester wool, or 9 mm prefabricated panels, one obtains great ease of on-site installation, suitable maintenance, and the possibility of replacement in case of leakage or breakdown.

These porcelain stoneware and conductive paste panels are ideal for thermal conditioning. In fact, when equipped with high thermal conductivity and effusivity, their thermal capacity is similar to that of common plaster panels (Table 1). Although in the case of metal roof sheets, the values of these parameters are four times lower, tests that assess the minimum time until emission temperature is reached turned out ten minutes for plaster and low thickness porcelain stoneware (Fig. 3), and five minutes for the metal ceiling. Prototypes were recently made and fixed to a wall in two office rooms at the University of Alicante. The building has an all-water air conditioning system. A management substation was installed in the system, and existing connections were redirected to the fan-coil to ensure distribution to four 2.5 × 1 m radiant panels. Currently, hydrothermal comfort and emission power are satisfactory. These empirical data were applied to a single-family house located in Alicante on the Spanish Mediterranean coast, with excellent results regarding comfort and the reduction of energy consumption [33]. Large-format TCP ceramic panels also offer other advantages over plaster and steel sheet finishes: they are inert regarding chemical actions or oxidation and degradation by usage. Mechanical resistance is better too: the wall application can be reinforced by adhering two ceramic pieces using a butyral, or fibreglass reinforced polyester with a thickness of 3 + 3 mm. In the case of false ceilings, the low-thickness porcelain stoneware is light and does not suffer deformations or damage during maintenance operations. The aesthetic possibilities are huge, with an abundant choice of finishes, including image printing using the Inkjet technique [34,35] before the firing process.

2. Application of TCP panels in the University of Alicante Museum

The University of Alicante Museum (MUA) has a range of different volumes. Some rooms are semi-buried, and the rooftop is covered by a 20 cm thick water bed. The present study focused on the museum's main hall or "Cube": a detached and flexible volume whose enclosure is finished with bakelised wood panels based on phenolic resins, measuring 63 × 22.5 × 9 metres (Fig. 4). The configuration is based on passageways throughout its perimeter allowing circulation over three levels for maintenance tasks. Underroof circulation also takes place through 8 passageways connecting the two main façades. This buffer space is used for all the building's lighting, air-conditioning and water-evacuation installations. The roof includes 7 giant skylights with orientable external aluminium blades. The perimeter on the ground floor is made of simple glass, with MD panel-based protection.

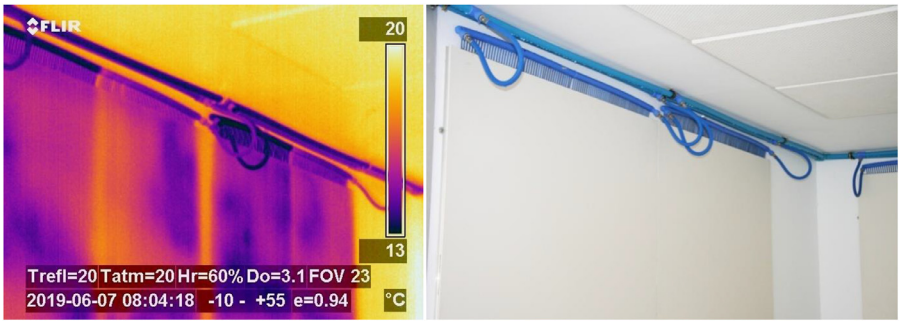

Fig. 3. Thermographic image of the TCP panels in summer.

Fig. 4. View of the Museum of the University of Alicante (MUA).

The interior enclosure consists of white-lacquered MD panels glued with polyurethane cord on timber frames and screwed onto a steel tube substructure (Figs. 5 and 6). The outer enclosure is made up of sandwich type panels with rock-wool insulation, a phenolic outer panel, an MD interior panel, and timber frames on the periphery. The enclosure was damaged by humidity, solar radiation and heat differentials caused by thermal bridges due to discontinuity in the insulation material. In 2010, the enclosure underwent an energy rehabilitation. A total of 3 cm of projected polyurethane was applied to the existing skin, and a ventilated facade was created, taking advantage of the existing metal substructure, with latest generation phenolic panels.

The current air conditioning system of the MUA's "cube" hall is an all-air system, with a split heat pump system located inside the conduits in the top part. Primary air is distributed through fiberglass conduits. The air is renewed by means of rooftop inlets, through manholes with drains that avoid the inlets from protruding above the rooftop plane.

The present study was based on the hypothesis of replacing the MUA's "cube" hall flooring with TCP panels, thus introducing a radiant floor cooling and heating system. In this way, the air conditioning system would be replaced by a radiant floor system by means of hot water distribution in winter and cold water in summer, which also requires installing a fan-coil dehumidification system in the conduits. For this purpose, prefabricated panels would be used with pieces of latest generation porcelain stoneware 20 mm thick (Figs. 7 and 8). Hot or cold water would be distributed using a 32 mm-outer diameter PPR pipe system, embedded in the flooring in 180 × 110 mm metal pipes. TCP panels, containing 3 mm PPR capillary tube mats, would be connected with flexible hoses and click & cool connections.

1. Large-format porcelain stoneware piece. 300 × 100 × 2 cm.
2. Adhesive layer. Beka Thermal Conductive Paste V. WLP. 1. Thickness: 6 mm.

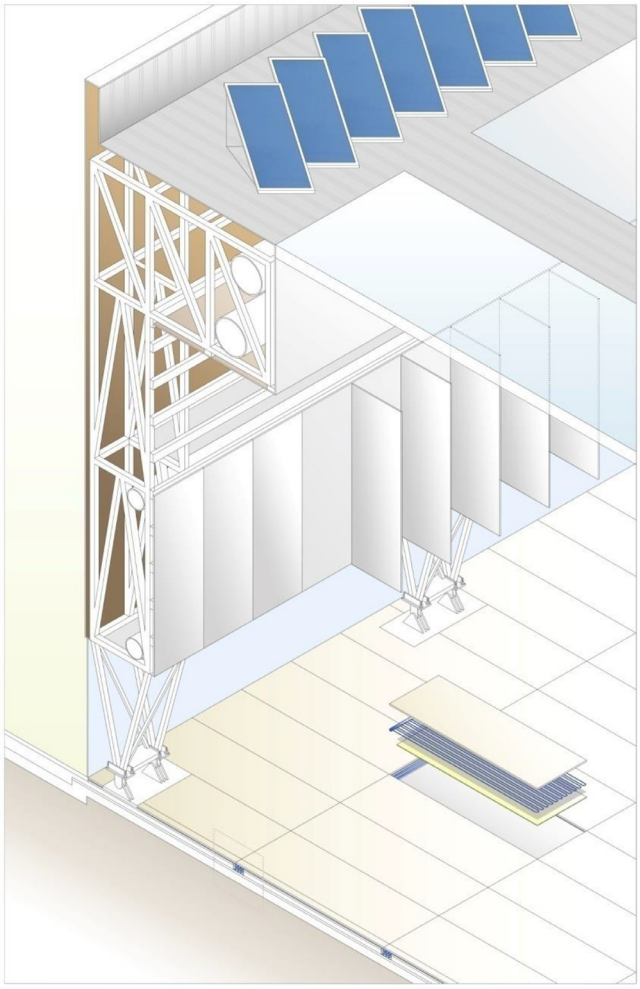

Fig. 5. Patent reference P201001626. Thermal Ceramic conditioning Panel application in the MUA.

3. PPR capillary mat. Diameter: 3 mm. Separation: 10 mm.
4. Polyurethane foam thermal insulator. Thickness: 10 mm.
5. Regulatory layer. Self-levelling cement mortar. Average thickness: 10 mm.
6. Coating of screed: expanded clay. Thickness: 80 mm.
7. Aluminium channels to pass the PPR distribution pipes through.
8. PPR distribution pipes. Diameter: 32 mm.
9. Thermal insulator. Type IV expanded polystyrene. Thickness: 40 mm.

Fig. 6. View of the MUA's main hall interior.

10. Reinforced concrete slab with electrowelded mesh 150 × 150 mm. Thickness: 150 mm.

3. Method

3.1. Comfort assessment of TCP panels applied to floors, walls or ceilings

We analysed the comfort levels and annual energy demand of different types of TCP panel applications. Five viable placement options (OP 2-OP 6) are shown in Fig. 9: on opposite walls with a continuous surface; on orthogonal wall panels to the wall surface; on a continuous suspended ceiling, in baffle-type vertical ceiling panels; and in radiant floor panels. The white porcelain stoneware panels would alter the aesthetics in most cases, although they would allow natural light to come in a similar way to the way light enters at present. Only OP 6 would lead to a variation in the effects of natural light, as the panels are placed orthogonally to the ground floor's perimeter glazing and the existing MD panels would be dispensed with.

Using the Design Builder tool, we proceeded to simulate thermal behaviours and calculate energy demands, both in the MUA's current state and with possible envelope renovations [36]. The application of TCP thermal ceramic panels to the walls and ceilings inside the MUA's "Cube" room had been simulated previously. Results were published in 2014 and 2016 [26,37]. The impact of the isolation of the new ventilated facade and the reduction of thermal bridges led to a drop in annual energy demand of 12% and 6%, respectively [38]. Results for this parameter were obtained with operating temperatures of 21 °C in winter and 24 °C in summer, an occupancy of 0.15 people per m^2, and air ventilation of 1 ren/h. The application of thermal ceramic panels to walls and ceiling was also compared to the air conditioning system. The results for user thermal comfort were equally satisfactory in summer and winter regimes, as the radiant system was capable of dissipating, by means of radiation and convection, around 60 W of heat per square metre of body surface in the summer regime [26].

To compare the energy efficiency of the different radiant systems proposed with all-air conditioning systems, similar user comfort levels were established. The objective of the research was not to evaluate users' degree of comfort in the scenarios under study, but the value of the operating temperature T_o itself, to compare the energy consumption of the two systems and the 6 options. The Fanger methodology was followed based on the simplification of the ISO 7730: 2005 standard [39]. We believed it was unnecessary to follow Fanger's entire calculation methodology of predicted mean vote (PMV) and predicted percentage dissatisfied (PPD) [40], which would constitute in itself a separate highly complex study due to "local thermal discomfort" conditions: air currents, vertical temperature difference, or the existence of cold or hot ceilings, walls or floors (asymmetry of the radiant temperature). We followed the guidelines of Spain's RITE IT 1.1.4.1.2. regulations, in accordance with the CTE. Considering the values of 1.2 met, 0.5 CLO in summer and 1 CLO in winter, and operating temperatures between 22.42 °C and 23.66 °C, following ISO 7730, PMV values between −0.66 and −0.17 were obtained, that is, a "slightly cool" thermal sensation. The PPD values ranged between 6.79% and 14.86%.

To do this, the operating temperature parameter T_o was approximated and a similar relative humidity RH was established in all scenarios. T_o can be defined as "the uniform temperature of an imaginary enclosure in which an occupant would exchange the same amount of dry heat by radiation plus convection as in the same actual environment, without taking into account latent loads" [41]. The user's feeling of comfort would depend on heat exchange by convection and radiation with the environment's surfaces and objects, on the water vapour's capacity of emission to interior air through skin perspiration and breathing, as well as the quality of the interior air. We analysed the parameters that directly affect feelings of comfort, i.e. mainly: the air's dry temperature, its relative humidity, the speed of the surrounding air, and the surface temperature of each of the premises' walls [42]. The speed was set at 5 cm per second for the TCP panels, obtained in situ in the monitored offices, and 15 cm/s in the case of the all-air installation, as the average value of the occupancy area obtained in situ. The heat losses by convection and radiation were obtained through the expressions:

$$q_{cvi} = h_c(T_i - T_a) \quad \left(W/m^2\right) \tag{1}$$

$$h_c = 14.11 \cdot v^{0.24} \ (W/^\circ C) \tag{2}$$

$$q_{rdi} = h_r(T_i - T_{rm}) \quad \left(W/m^2\right) \tag{3}$$

$$T_{rm} = T_1 \cdot F_{P-1} + T_2 \cdot F_{P-2} + \cdots + T_N \cdot F_{P-N} \tag{4}$$

Fig. 7. Different layers of the Ceramic Thermal Conditioning Panel applied to the MUA floor.

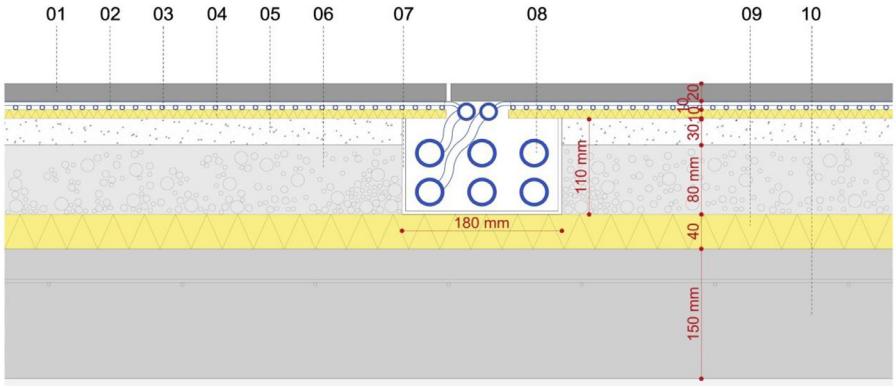

Fig. 8. Ceramic Thermal Conditioning Panel applied to the MUA floor.

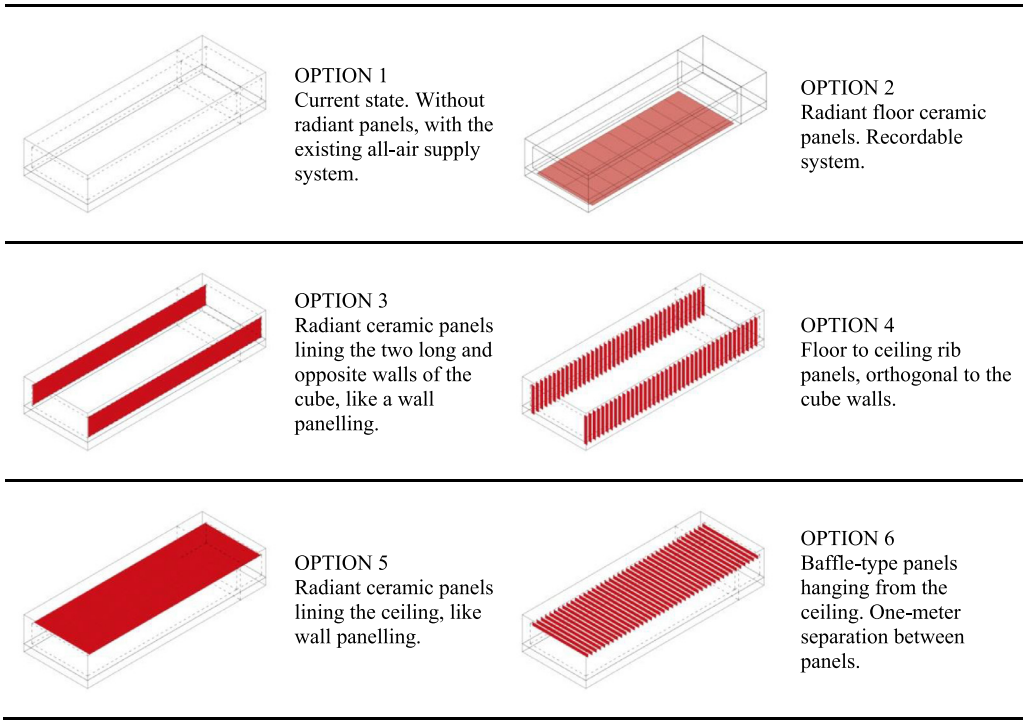

Fig. 9. Different placement options of the thermal ceramic panels.

The h_c convection factor is directly related to air speed. It usually has an average value of 3.5 W/m^2 °C, with an air speed of 0.1 m/s. This factor was corrected as a function of air speed in both HVAC systems. The radiation loss coefficient h_r takes on approximate values of 4.7 W/m^2 °C with an estimated human body temperature of T_i of 30 °C.

To conduct the research based on similar user comfort levels, in addition to the operating temperature T_o in the different scenarios, the values of heat loss by radiation and convection (q_{rdi} and q_{cvi}) were quantified and unified. To proceed to evaluate q_{rdi} and q_{cvi} in the MUA hall, we obtained, through monitorisation, the surface temperature data, indoor air temperature and air speed of the current state (that is, in OP 1) for the convective system, and equivalent data for the radiant systems options OP 2-OP 5 by means of Design Builder simulations [10,26]. Based on these premises, we proceeded to calculate the form factors for radiant energy for the 6 options, taking into account an individual in a standing position in the centre of the room, and subsequently the average radiant temperatures according to the expression (4) [43,44]. Values q_{rdi} and q_{cvi} of heat losses by radiation and convection were quantified for one individual, in each scenario under study. The sum of both values proved to be very similar whether in the case of convective systems or radiant systems. To conclude, given that the usual sensible heat emission values of a user walking slowly are 90 W [41], the best-performing options were: OP 1, OP2, OP 5 and OP 6.

3.2. Calculation of the operating temperature t_o for the 6 options

Once the h_c convection coefficients and the h_r radiation losses were determined with sufficient accuracy, we proceeded to calculate the values of operational human body comfort temperature T_o, according to the expression (5):

$$T_o = \frac{h_r T_{rm} + h_c T_a}{h_r + h_c} \tag{5}$$

By interpreting this expression, we can understand how radiant surface heating systems work. An individual's feeling of comfort in enclosed spaces, applying prior control of relative humidity and air speed according to the Spanish Regulations on Heating Installations in Buildings (the RITE)— i.e. between 40 and 60%, and 0.15 to

Table 2
Calculation of annual energy demand to calibrate the Design Builder model.

Building occupancy	Fresh air (acH)							Actual energy consumption
	0,176	0,275	0,353	0,775	1059	1250	1765	
People	Annual energy demand (kWh/m^2 y)							(kWh/m^2 y)
700	170,14	175,89	185,89	191,58	201,58	207,31	217,31	139,31
600	154,89	168,25	178,25	183,96	193,96	198,69	208,69	139,31
500	150,00	160,61	170,61	176,33	186,33	190,06	200,06	139,31
400	146,78	152,50	162,50	168,22	178,22	180,95	190,95	139,31
300	138,57	144,29	154,29	160,11	170,11	175,84	185,84	139,31
200	130,56	136,28	146,28	152,02	162,02	165,73	175,73	139,31
100	122,45	128,17	138,17	143,89	153,89	159,62	169,62	139,31

Fig. 10. Temperature and humidity sensors and analysers EL-WiFi-TC and TH.

0.24 m/s according to the winter or summer regime, respectively—, depends on the surrounding air temperature and the surface temperature of the space's walls. In addition, comfort levels are higher because indoor air speed in summer is three times lower in radiant systems. As shown, in the case of the MUA, the indoor air temperature in summer was 2–3 °C higher in radiant systems compared to convective systems (Table 2).

3.3. The MUA monitoring system

As indicated above, the MUA was monitored during the complete year 2014 cycle, applying over 30 sensors of surface temperature, indoor and outdoor air temperature, relative humidity, pyranometer, indoor air speed, etc. We chose a wireless monitoring system. Surface temperature sensors were connected to small analysers, model "EL-WiFi-TC-Thermocouple Probe Data logger" (Fig. 10). A series of analysers "EL-Wifi-TH, Temperature and humidity data logger", with built-in indoor air temperature and relative humidity sensors, interpreted the recorded data [45] and sent wifi signals to a "RouterOS" model router [46]. That router was connected to a laptop computer that processed the received information. By installing the "EasyLog WiFi Software", the data sent by the analysers was received and stored on the hard disk. The data was sent daily to a virtual disk; the information could then be accessed using a personal code from any network point. In addition, a small station was installed on the roof of the building with sensors for outside air temperature, relative humidity, and a pyranometer to measure solar radiation (KIPP Model CMP3 ISO second class).

To calibrate the model and to adjust it to real thermal behaviour, we used the climate file obtained on site and validated it using the climatological data recorded by the weather station of the Climatological Laboratory of the University of Alicante. We also modified the value of air infiltration through the enclosures, using the Design Builder simulation tool. We thus adjusted the annual energy demand obtained according to real energy consumptions provided by the Vice-Rectorate of the Campus and Technology of the University of Alicante. Average energy consumption over the 2010–2014 period was 203,050 kWh/year. After deducting the lighting consumption value —2.8 kWh/m^{2}y—, a value of 197.5 MWh/yr was obtained for the existing all-air conditioning system. The same methodology was followed to adjust indoor surface temperatures and indoor air temperature. Fixing the set temperature at 21 °C in winter and 24 °C in summer facilitated the calibration process, added to the fact that users could not adjust the air conditioning parameters themselves. The activation time of the all-air installation was from 9 am to 8 pm Monday to Friday.

The scale and construction characteristics of the MUA's access doors prevented us from performing the Blower Door test in the MUA. To obtain the mean calculated value of the building's air infiltration—a parameter that is difficult to quantify—and to perform the simulations in Design Builder, we resorted to recent research results, using the test measurements of similarly constructed buildings around Alicante [47]. We then proceeded to make Design Builder simulations with an all-air supply system, and determined that the actual volume of renewal air was 0,353 acH. Once these prior values were obtained, we followed the protocol of the UNE-EN-ISO 13,790:2011 standard [48], applying the value obtained in the 50 Pa (n_{50}) pressure test. The result was 0.842 acH, a high value for a building of this nature, with a low form factor value. This high infiltration value was due to the silicone joints between phenolic panels having deteriorated over the years. The same occurred on the ground floor: the simple Stadip glass silicone joints had also deteriorated. The rooftop also presented a high infiltration value as it had been executed dry, with deficient joints between the sandwich panels and the skylights. The annual values obtained for annual energy demand, based on the occupancy rate, air renewal rate and air infiltration across various scenarios are shown in Table 2 and Fig. 11. Convergence with the real value of the energy consumption obtained from the MUA's electric meter consumption data (139.31 kWh/m^{2}y) occurs with an average occupancy of approximately 100 people, an air renewal rate of 0.353 acH and air infiltration of 0.842 acH. At a value of 0.353 acH, the air renewal would be of 4502 m^3/h out of a total of 47.233 m^3/h of supply air, that is, 9.5%, which coincides with the MUA's air conditioning project.

The Thermographic camera ThermaCam P 25 by Flyr was used to detect thermal bridges [49], and their effects were substantially mitigated after the enclosure was renovated with a ventilated façade system. The continuous projection of 3 cm polyurethane foam reduced the thermal transmittance U values and linear thermal transmittance Ψ in joints, singular points and structural points [50,51]. The quantification was made using the AnTherm software: load gains or losses due to thermal bridges were estimated at 3.5% of total thermal loads [52] due to thermal transmittance U of the

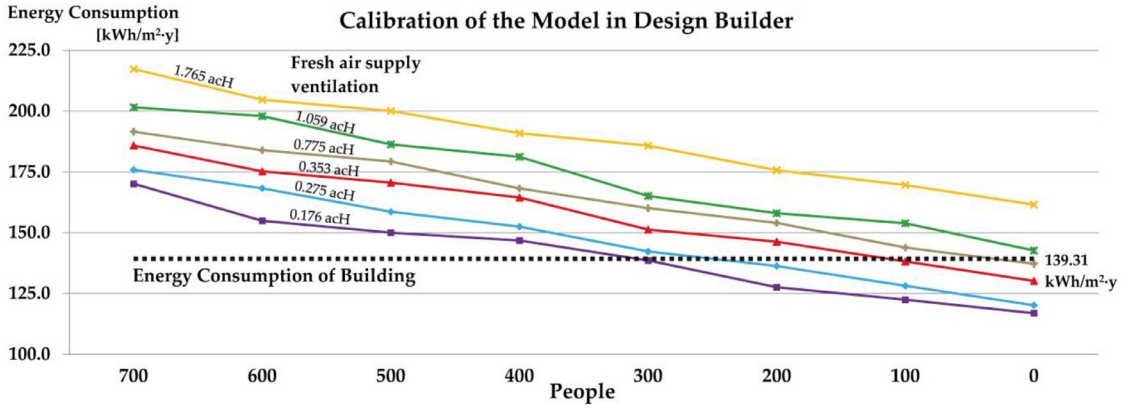

Fig. 11. Calibration of the Design Builder model. Occupancy settings and ventilation air.

enclosures, a value that was similar to that obtained in previous studies [53,54].

3.4. Annual energy demand values

Spanish regulations on energy efficiency in buildings make it compulsory to fill out the DB-HE technical document on energy saving, which is part of the Technical Building Code (or CTE by its Spanish acronym) [44,55]. The regulation requires you to apply the standardised tool, Lider-Calener HULC [56], to architectural projects. The instrument, however, has notable shortcomings compared to other simulation instruments such as Design Builder or TRNSYS. These latter tools allow adjusting to the actual use of the building, such as opening or closing windows according to time slots or using the enclosures' thermal inertia for thermal comfort and reducing energy demand through phase change materials [57]. HULC is much more limited, it is oriented towards favouring certain energy policies that are not always justifiable [58]. HULC does not allow to introduce certain types of bioclimatic techniques either. For this research, the Design Builder tool was chosen for its proven reliability by means of the EnergyPlus calculation engine.

3.5. Incorporation of solar thermal panels

As previously commented, the TCP system distributes hot and cold water at moderate temperatures, making it easier to use alternative energies such as solar energy. Solar thermal panels could be placed on the MUA's rooftop; they work by heating the system's water in winter or cooling it in summer by means of an absorption cooling system based on BrLi lithium bromide [59,60], or ClLi chemical energy (solar cold) [61,62]. The levels of solar radiation could be obtained at any time of the year using the data collected by the pyranometer (KIPP Model CMP3 pyranometer ISO second class) in the monitoring system. This would allow quantifying the energy fed to the system according to the installation's performance. This energy would be contributed indirectly in the heating regime, when temperatures reach between 20 °C and 35 °C as the water would be preheated prior to its passage through the air-water heat pumps; it would be directly contributed when the tank's capture temperature is between 35 °C and 50 °C. In summer the energy would be contributed by absorption or solar cold. Therefore, taking into account the systems' usual performance, and a breakdown of each component's energy consumption, this system, i.e. option 7 (OP 7) can be compared to the radiant floor system (OP 2) and the current all-air system (OP 1).

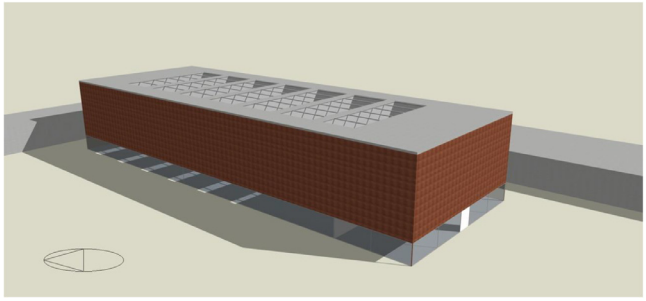

Fig. 12. Model of the MUA in Design Builder.

4. Results

To perform the MUA simulations of thermal comfort, adjustment of operating temperatures T_o using the expression (5), thermal behaviour and annual energy demand, the following recorded data were introduced into the Design Builder tool (Fig. 12):

1. The winter period covers 1 December to 30 April, and summer covers 1 May to 30 November. These are the usual weather conditions of San Vicente del Raspeig (Alicante) where the University of Alicante is located.
2. The temperature of indoor air is 21 °C in winter and 24 °C in summer. RH remains at 50%.
3. Occupancy, according to the standard CTE calculation of air renewal, is of 709 people, 0.5 people per m^2, since the DSI fire protection values must be applied. A value of 2.5 acH air renewal is required, with 12.5 litres per second and per person. This high value was adjusted in Design Builder's model calibration, according to the actual consumption of energy obtained from the building's meter, with an average real occupancy of 100 people at peak visiting times, with a result of 0.353 acH of air renewal.
4. Air infiltration through the enclosure was high, although it was moderated thanks to the application of continuous polyurethane foam during the MUA's 2010 rehabilitation. As indicated, the quantification was performed using a comparison with the Blower Door test carried out in similarly constructed buildings around Alicante [47]. The adopted value was 0.864 acH. The test was conducted in accordance with European Regulation EN 13,829, using BlowerDoor Gmbh MessSysteme Für Luftdichtheit equipment.
5. We estimated load gains or losses due to thermal bridges at 3.5% of total thermal loads [52] by *U* thermal transmittance of the enclosures [63,64], which were obtained on site by means

Table 3
Summary of parameters introduced in Design Builder's simulation model.

Parameter	Data introduced	Other introduced data
Hours of operation, activity and occupancy	8 am to 8 pm	
Climate equipment operating hours	7 am to 8 pm	
Running of the air conditioning system from Monday to Friday	5 days/week	
Performance of the weekend climate control system	Maintenance	
MUA occupancy density	0.07 person/m^2	100 persons MUA
Occupancy of the passageways "Light plant room"	0.01 person/m^2.	8 persons
Metabolic factor: "Standing/walking" option	1,20	
Clothing values (CLO)	winter CLO=1,00	Summer CLO=0,50.
Load due to general lighting	300 lx	10.20 W/m^2
Gains from office equipment	1.52 W/m^2	
Passageways: "light plant room"	No conditioning	No air renewal
Internal air temperature setpoint *Ti* (cooling)	24 °C	
Set internal air temperature *Ti* (heating)	21 °C	
Indoor air maintenance temperature *Ti* (cooling)	28 °C	
Internal air maintenance temperature *Ti* (heating)	12 °C	
Relative humidity of the indoor air	50%	
Air renewal rate	0.353 acH	
Air infiltration through the envelope	0,842 acH	n_{50} = 8,42 acH
Skylights: protection of horizontal aluminium slats	Total darkening	No thermal break
Joineries	Aluminium	No thermal break
Option of existence of Sanitary Hot Water (SHW)	Deactivated	

of the multifunction instrument KIMO TM210 by Testo [65,66]. A ThermaCam P25 thermographic camera was used to detect them [49]. Evaluations were made as mentioned using the An-Therm tool [67].

6. The large skylights were considered to be in their usual state; their interior aluminium blades were completely closed to the passage of solar radiation.
7. The ground floor perimeter glaze was protected with continuous MD wood panels separated by 1.40 m, preventing direct interior solar radiation.

Table 3 shows the introduced parameters.

The schematic diagram of the capillary tube mats project was introduced into the Design Builder model (Fig. 13). The surface temperatures of the TCP panels were then pre-set to 17 °C, to avoid the risk of surface condensations. We also introduced the climate file relating to external air temperatures, relative humidity, and solar radiation levels by pyranometer throughout a complete one-year cycle, obtained for Alicante in previous studies [26,68]. Lastly, the walls' surface temperature was corrected, and the infiltration value was adjusted to 0.342 acH, so the model was calibrated by adjusting the air and wall temperatures to the monitoring values [46]. We also applied the dehumidification of the ten fan-coils, with a total power of 25 kW and an energy consumption of 27,854 kWh/yr.

4.1. Operating temperatures T_o

Graphs 1 and 2 show the summer temperature values on 2 August 2015. They were obtained by monitoring the building, and via Design Builder simulations of the TCP panel radiant system options. The following temperature values are shown: outside air; indoor air temperatures of points 1 and 3 in the occupancy zone for the current convective system or OP 1 and for the radiant floor panel system or OP 2; and indoor air temperature values in cases where the air conditioning system is not operational.

As can be seen in Table 4, the T_o operating temperatures, obtained through the expression (5), come close to the 23 °C value introduced in the Design Builder simulations for the summer regime, as required by the RITE. In these systems, by providing a large surface focal point on the floor, ceiling, or wall, the surface temperatures of the heat or cold-emitting focal point become more moderate than in hot water radiator installations or chilled water systems. In this way, the same level of emission power is achieved as in convection systems, and at a similar operating temperature. As we will see, this difference generates substantial energy savings, and allows using alternative energies, such as solar [69,70], airothermal or geothermal energies [71,72].

Table 4
Calculation of operating temperatures in summer for the six options.

	v h_c=14.11$v^{0.24}$	h_c	T_a	h_r	T_{rm}	T_o
	m/s	W / °C	°C	W /m^2 °C	° C	°C
OP 1	0.068	7.402	22.11	4.70	24.45	23.02
OP 2	0.036	6.354	25.63	4.70	20.05	23.26
OP 3	0.035	6.311	24.37	4.70	22.70	23.66
OP 4	0.026	5.877	24.10	4.70	22.37	23.33
OP 5	0.032	6.177	24.28	4.70	19.98	22.42
OP 6	0.039	6.477	24.10	4.70	20.34	22.52

To conclude this comparative analysis of radiant floor TCP panels, we can fairly say that optimal comfort would be reached in the winter regime, with an adequate temperature gradient in the occupancy area, and, as we will see, significant energy consumption reductions would be obtained. When operating with air temperatures at around 2 °C below that of convective systems, the air does not dry up significantly and a humidification system is not required. In summer, the system would produce a satisfactory temperature gradient, cooling the indoor air in occupancy areas, as well as the glazed walls. The biggest downside of ceiling applications in OPs 5 and 6 would be the risk of floor surface condensation, which would make the space impracticable. The indoor air would have to be dehumidified with a fan-coils system located in the conduits and the water distribution temperature in the capillary mats would have to be limited by means of a condensation control sensor [10].

4.2. Annual energy demand and comfort conditions

Once the air renewal rate parameters above were obtained according to the CTE —air infiltration, surface temperatures, occupancy, etc. — and we had calibrated the model, we simulated the MUA's behaviour according to the six options mentioned above. The thermal loads, solar gain by glazing, internal thermal loads, and summer, winter and annual energy demands were compared in the case of the 6 options described above, plus the possibility

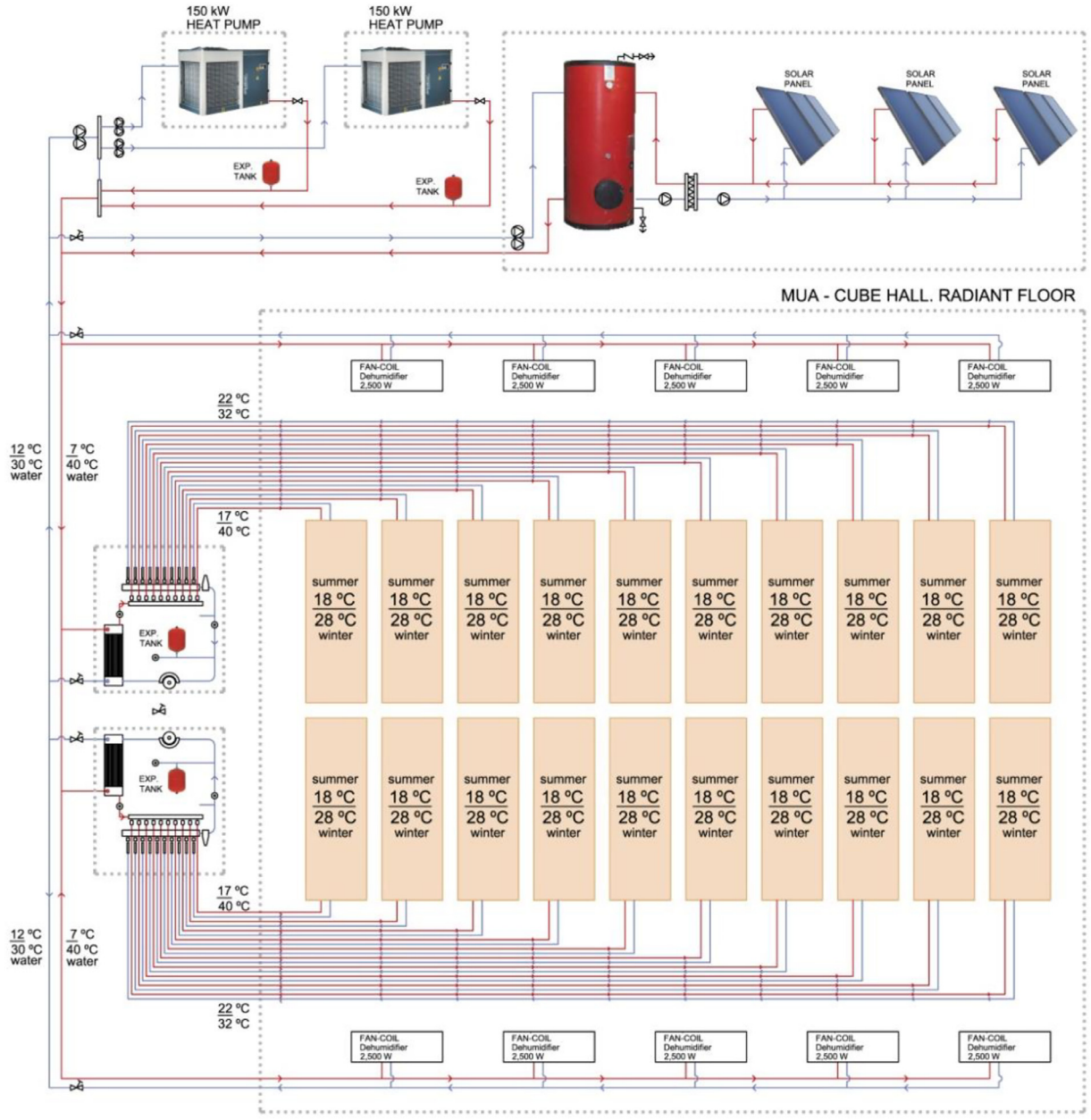

Fig. 13. Schematic diagram of the installation modelled in Design Builder.

of incorporating solar thermal panels on the rooftop (OP 7). Investment amortisation periods were estimated for three different scenarios (SC) relating to the above options:

SC 1. All-air installation based on reversible air-air heat pump split system, model XPOWER VRF 2 tubes (38VT-168HTEE) and air conditioner 39SQ flow rate 1.8 m^3/s by Carrier, with 148 kW cooling power and 162 kW heat power. Condenser and climate control in the MUA's conduit. This scenario corresponds to OP 1.

SC 2. Installation of PPR capillary tube mats, in TCP panels, with air-water heat pump model Aquasnap 30RQSY039-160 by Carrier, 148 kW cooling power and 162 kW heat power similar to OP1, distribution of water to two distribution substations located in the MUA's conduits, and water distribution in the secondary circuit through 24 independent PPR circuits 32 mm in diameter per paving, and ten fan-coils strategically located for air dehumidification, each with a cooling power of 2.5 kW. This scenario corresponds to OP 2.

SC 3. Installation of PPR capillary tube mats similar to SC 2, with the same heat pump as above, and the ten fan-coils for air dehumidification, with a system of 230 m^2 of solar thermal panels, with chemical energy LiCl cooling (solar cooling), providing alternative energy to the system. This scenario corresponds to OP 7.

Table 5 shows the results regarding thermal loads and solar gains [73] obtained in Design Builder for the first three options for OP1- OP2. They can be observed to be very high, largely boosted by the presence of huge rooftop skylights lacking protection, despite having been later covered with sandwich panels. Using TCP panel radiant systems would reduce these thermal loads by 18% in the case of the radiant floor in OP 2, and by 17.2% in the case of OP 3. The most decisive factor was the T_i indoor air temperature's

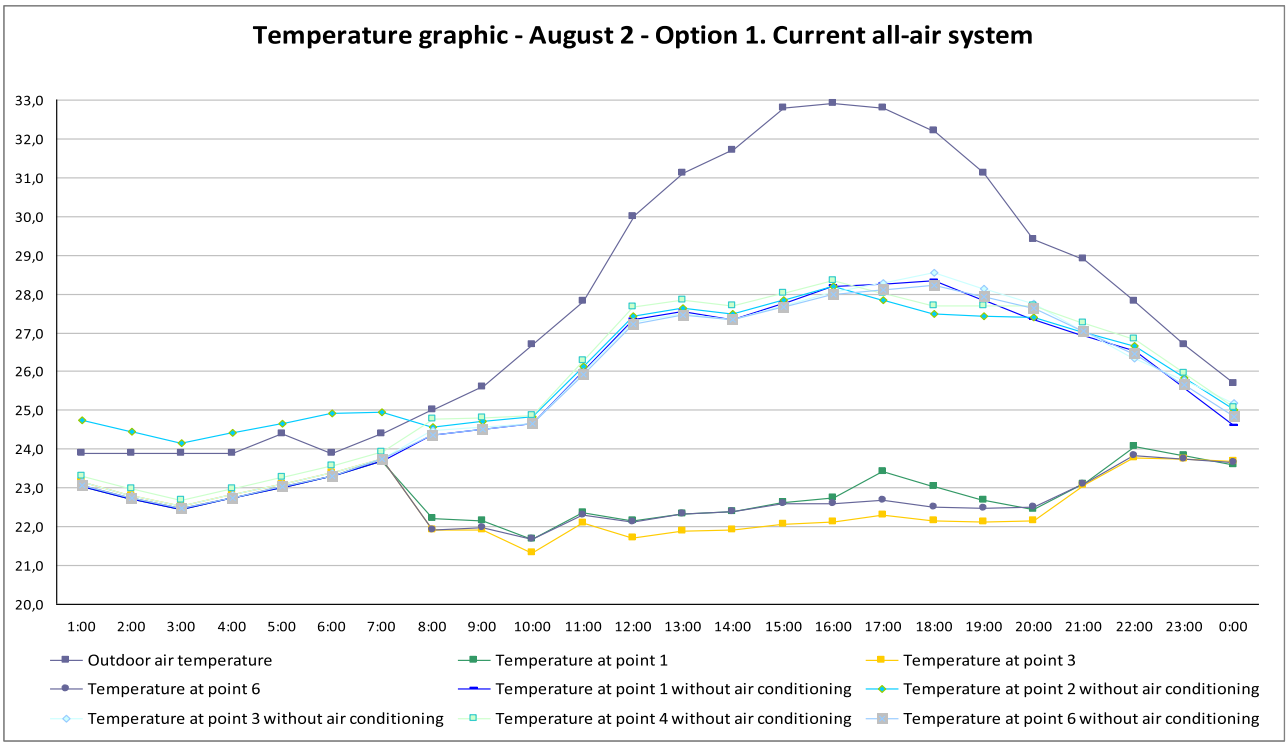

Graph 1. Temperature of indoor and outdoor air in summer, in the case of an all-air system and no conditioning.

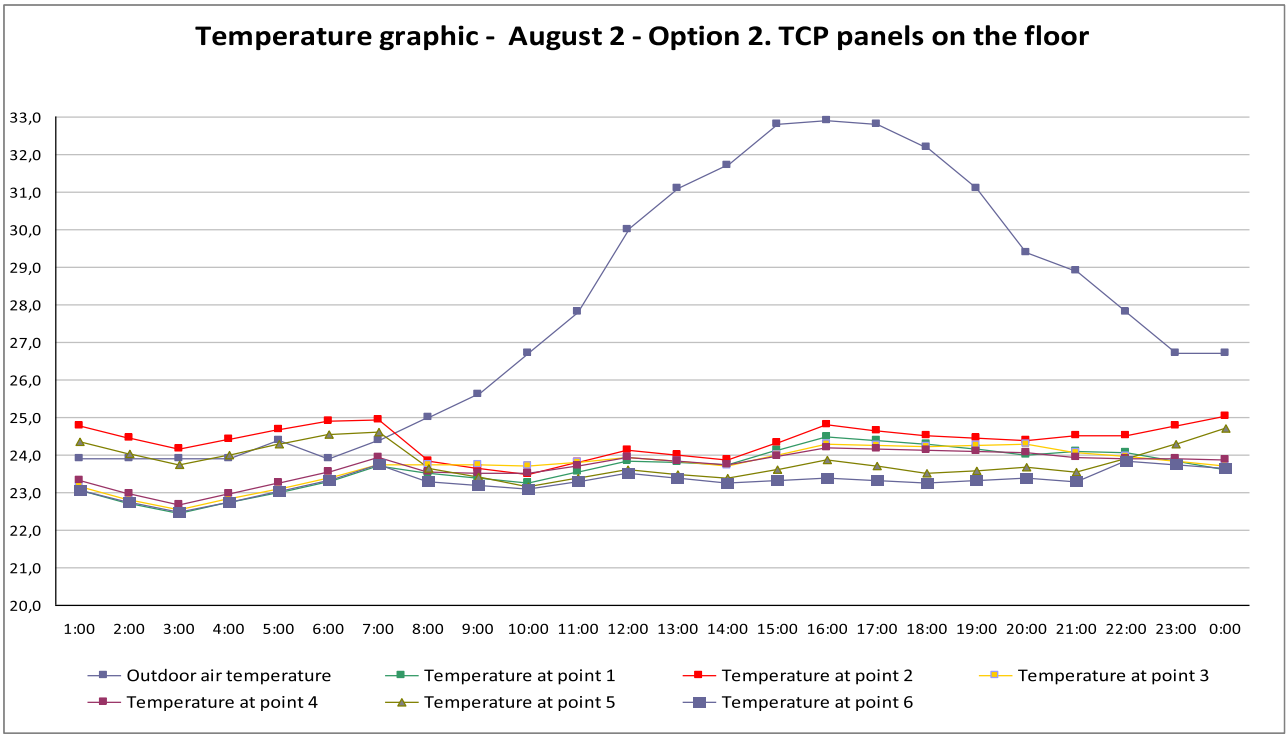

Graph 2. Temperature of the indoor and outdoor air in summer, in the case of a radiant floor TCP ceramic panels system.

increase in summer and drop in winter, substantially reducing heat flows by *U* transmittance through all exterior walls.

Table 6 shows the results obtained by simulation regarding summer, winter and annual energy demands for the seven options OP 1-OP 7. The values were similar to those usually obtained for office buildings, for which 30% and 35% energy savings compared to convective systems were accredited in Central Europe [10]. They are somewhat inferior because the outside air RH is higher on the Mediterranean coast. The MUA's annual energy demand was 130.83 kWh/m^{2}y for the currently installed all-air system, and 98.25 kWh/m^{2}y for the system of TCP thermal ceramic floor panels (OP 2). The energy savings obtained amounted to 24.91%. These reductions are similar to those obtained in previous studies [74]. In the case of radiant wall or ceiling systems,

Table 5
Calculation of loads and energy demands. Current state, radiant floor OP2 and radiating walls OP3.

	OP1 MUA 2000		OP2 TCP radiant floor		OP-3 TCP radiant wall	
	Summer Wh/m²yr	Winter Wh/m²yr	Summer Wh/m²yr	Winter Wh/m²yr	Summer Wh/m²yr	Winter Wh/m²yr
Enclosure						
Glazing	15,733	20,069	8716	18,341	9138	18,478
Walls	1689	216	814	251	1025	228
Floors - ground	−1506	6367	−1403	5002	−1483	5327
Partitions	0	0	0	0	0	0
Rooftops	5279	7115	2452	4835	2874	4972
Outdoor floors	310	167	296	138	307	148
Infiltration	12,193	21,532	6393	17,031	7387	17,145
	36,119	**54,211**	**17,268**	**45,599**	**19,248**	**46,298**
Loads						
Lighting	2414	2833	2414	2833	2414	2833
Equipment	3766	2658	1219	1050	1429	1301
Occupation	8956	6975	8956	6975	8956	6975
Solar gains	38,541	−25,637	38,541	−25,637	38,541	−25,637
	53,671	**−13,171**	**51,177**	**−14,779**	**51,387**	**−14,528**
	kWh/m²yr	kWh/m²yr	kWh/m²yr	kWh/m²yr	kWh/m²yr	kWh/m²yr
Primary energy	**89.79**	**41.04**	**67.43**	**30.82**	**69.62**	**31.77**

Table 6
Calculation of energy demands and CO_2 emissions of the 7 OP.

	OP 1	OP 2	OP 3	OP4	OP5	OP6	OP7
Energy demand in summer kWh/m²	89.79	67.43	69.62	70.15	71.14	70.95	35.91
Energy demand in winter kWh/m²	41.04	30.82	31.77	32.31	33.39	33.12	15.39
Annual energy demand kWh/m²yr	130.83	98.25	101.39	102.46	104.53	104.70	51.30
Annual CO_2 emissions in use stage	50,071.91	37,603.22	38,804.99	39,214.01	40,006.77	40,071.31	19,633.17
Percentage	**100.00%**	**75.09%**	**77.50%**	**78.31%**	**79.90%**	**79.55%**	**39.21%**

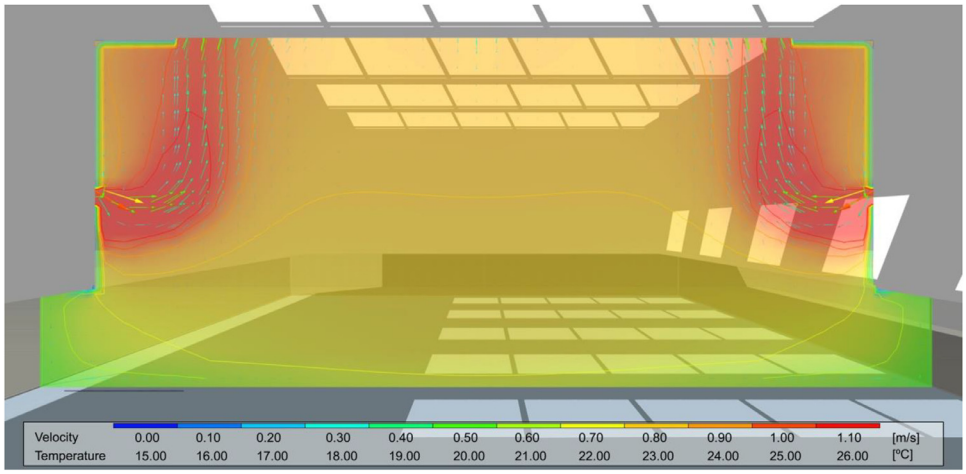

Fig. 14. All-air system. 1 February 2015. 9am.

energy demand reductions are somewhat lower. Figs. 14–17 show the temperature gradients produced by the simulation in the different housing spaces for both conditioning systems options OP 1 and OP 2. Homogeneous temperatures can be observed in the occupancy area for the TCP radiant systems, in addition to the fact that the indoor air temperature T_i was approximately 2–3 °C higher in summer and 2 °C lower in winter.

CO_2 emissions were also quantified during the MUA's usage stage, according to the electrical mix. We thus obtained an initial estimate of the resulting environmental impacts, based on the LCDN database [75]. According to this estimate, to produce 1 electric kWh, a total of 0.41 $kgCO_2$, 0.00122 $kgCH_4$ and 0.0000465 kgN_2O are released. Once users' final energy consumption was quantified for all three scenarios SC 1-SC 3, yearly CO_2 emissions could be quantified during the user stage. The system's primary energy consumption and CO_2 emissions were calculated using the factors of the Institute for Diversification and Saving of Energy (IDAE by its Spanish acronym) for 2010 [76], specifically: 2.21 MWh_p/MWh_f and 0.27 tCO_2eq/MWh (Table 6).

4.3. Incorporation of thermal solar panels

We will now analyse the energy savings that would result from incorporating a system of rooftop thermal solar panels to the radiant floor TCP panel conditioning system (OP 7) [77]. The solar radiation power data on the MUA rooftop were collected during the complete 2015 cycle, through a pyranometer installed on the MUA's rooftop. Graph 3 shows the radiation values obtained for the months of August and February. The daily average energy values collected each month are illustrated in Table 7. These values

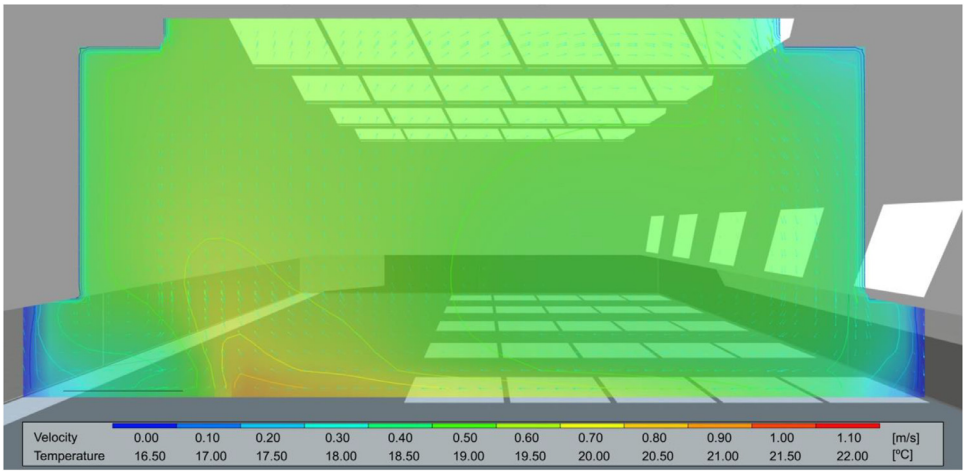

Fig. 15. Radiant system using TCP panels. 1 February 2015. 9am.

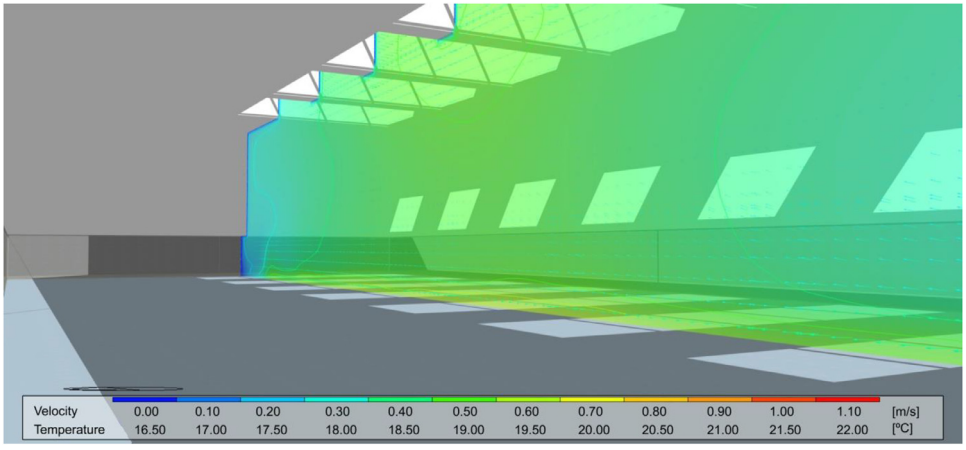

Fig. 16. Radiant system with TCP Panels. 1 February 2015. 9am.

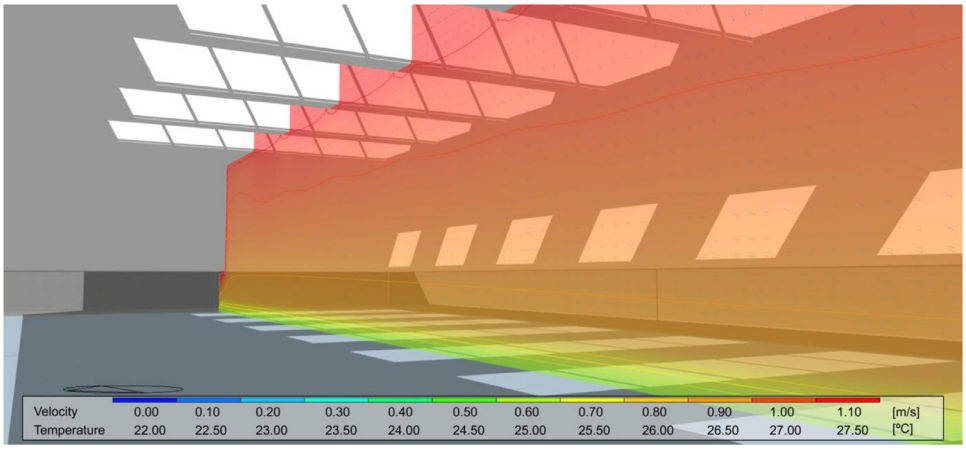

Fig. 17. Radiant system with TCP Panels. 1 August 2015. 3pm.

were contrasted with other sources and recent publications that collected such values in Mediterranean and Eastern Spain; correlated values were then obtained [61,78].

The installation was dimensioned according to the load calculations in Design Builder (Table 5). It was necessary to install 230 m^2 of thermal solar to achieve an annual conditioning energy demand of 98.25 kWh/m^2a, with an installation of two 150 kW heat pumps in cold mode in summer. According to previous calculations, these panels contributed 62.2% to the system during energy demand peaks in summer, at moments of maximum sunshine [72]. The performance of 230 m^2 of solar thermal panels, at a latitude of 38° latitude and a 45° inclination, was 71.4% [79]. Bearing in mind that the overall performance of the installation was 84.5% [80], the total energy contribution to the TCP panel system was 66,559 kWh/year. In winter, hot water is distributed to the capillary tube mats from the accumulation deposits of the solar panel

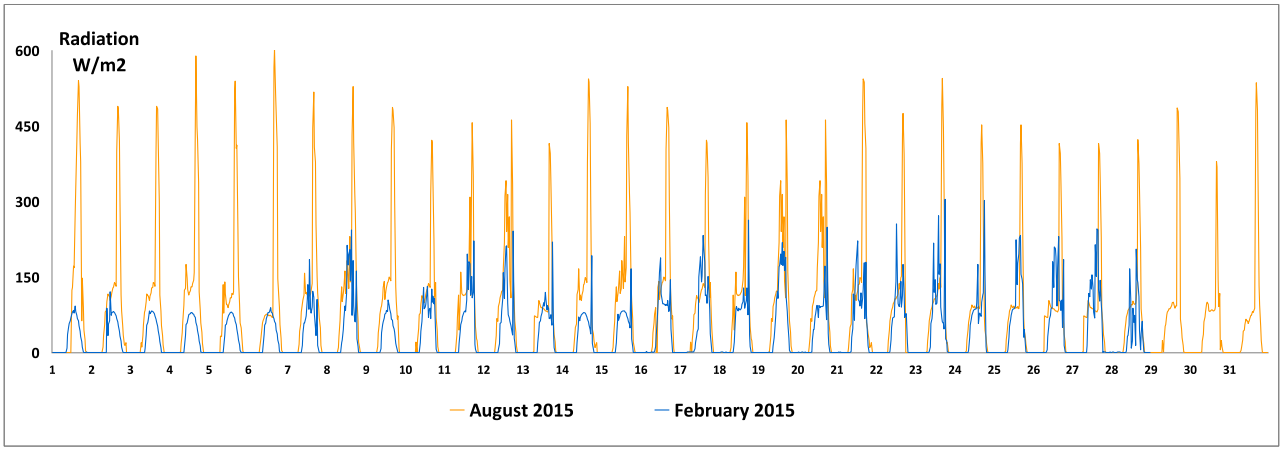

Graph 3. Solar radiation Values captured on site for the months of August and February 2015.

Table 7
Solar energy received per days, months and year.

Month	No of Days	Direct Irradiance (kWh/m^2 year)	Diffuse Irradiance (kWh/m^2 year)	Direct energy per month (kWh/m^2)	Diffuse energy per month (kWh/m^2)	Total energy per month (kWh/m^2)
January	31	1.66	0.95	51.46	29.45	80.91
February	28	2.31	1.18	64.68	33.04	97.72
March	31	3.03	1.67	93.93	51.77	145.7
April	30	4.30	1.83	129	54.9	183.9
May	31	4.65	2.26	144.15	70.06	214.21
June	30	5.40	2.25	162	67.5	229.5
July	31	5.56	2.17	172.36	67.27	239.63
August	31	4.65	2.17	144.15	67.27	211.42
September	30	3.79	1.66	113.7	49.8	163.5
October	31	2.69	1.30	83.39	40.3	123.69
November	30	1.84	0.97	55.2	29.1	84.3
December	31	1.44	0.83	44.64	25.73	70.37
Annual radiation				**1258.66**	**586.19**	**1844.85**

installation. In summer, cold water is produced through a solar cooling system with chemical energy storage by lithium chloride (LiCl). The latter can be subsequently cooled, if necessary in the heat pump, until the dehumidification fan-coil distribution temperature is reached in the heat pump (7 °C).

The results obtained from the Design Builder simulation were calibrated and corrected using the solar energy results obtained on site [33], contrasted with other studies on thermal energy in similar climates [61,81,82]. The energy savings produced in the system with respect to all-air systems amounted to 60.79%. These savings confirm that the radiant TCP panels system incorporating rooftop thermal solar panels constitutes a viable system. The energy consumption of the three analysed systems are broken down in Table 8 according to all equipment, pumps, circulators, fans, fan-coils, etc. and installation elements, including solar panel energy contributions.

As illustrated, the energy consumption of the all-air system with split heat pump machines for air distribution in SC 1 was 133% higher than that of the installation of water distribution to TCP panels in SC 2 and SC 3. Furthermore, it was 255% higher than that of SC 3 when installed with 230 m^2 of solar thermal panels on the rooftop. Energy consumption in SC 2 was 24.91% lower than that of SC 1 or the all-air system, for the reasons described in paragraph 1. Consumption due to dehumidification, with the two fan-coils of SC 2 and SC 3, was 43.09 MWh per year: the installation of TCP panels would thus, a priori, be more unfavourable than the all-air installation. However, globally, the system actually leads to substantial energy savings compared to SC 1 due to different factors. For example, the energy needed to transport water is drastically lower compared to that needed for air, and there is a drop in thermal load to the reduced thermal gap of the heat flow through the enclosures.

4.4. Investment amortisation approach

To complete this comparative analysis, we estimated how profitable the investments in technical installations that could be introduced in the MUA could be. We applied the UNE-EN 15,459–1:2018 standard [83] for the MUA's Life Cycle Cost (LCC) to the 3 scenarios under study. The Global Cost was applied using the expressions:

$$C_g(t) = C_l + \sum_j \left[\sum_{i=1}^{t} (C_{a,i}(j) \cdot R_{disc}(i)) - Val_{F,t}(j) \right] \quad (6)$$

$$R_R = \frac{R_{int} - R_i}{1 + R_i/100} \quad (7)$$

$$R_{disc}(i) = \left(\frac{1}{1 + R_R/100} \right)^i \quad (8)$$

Where:

C_l Initial investment costs
Ca Recurring costs
Rdisc Discount rate
i years

Table 8
Calculation of annual energy consumption of all the installation's elements compared to convective systems.

	SUMMER from 1 May to 30 November WINTER from 1 December to 30 April Occupation: 100 PEOPLE		SC 1 All air	SC 2 Floor TCP	SC 3 TCP +Solar panels
1	Effective Area	m^2	1417	1417	1417
2	Ceramic panels area	m^2		1390.5	1390.5
3	Maximum thermal load	W/m^2	80	75	75
4	Minimum fresh air flow rate	m^3/m^2 h	3.05	3.05	3.05
5	Thermal jump of the water in summer	k	6	4,6	4,6
6	System running time	h/year	4015	4015	4015
	Cooling pumps running time	h/year	1.800	1.800	1.800
	Total cooling running hours	h/year	620	205	205
	Total heating running hours	h/year	310	140	140
	Ventilation				
10	Supply air flow rate	m^3/hm^2	29.41	3.05	3.05
11	Supply air volume	m^3/h	41.674	4.320	4.320
12	Fan power	kW	11.27	1.21	1.21
13	Power consumption	MWh/year	175.65	19.80	19.80
	Comparison	%	100%	11,2%	11,2%
	Cooling pump				
14	Water flow rate	l/m^2 h	11.46	21.5	21.5
15	Volume of water	l/h	16,238.5	26,265	26,265
16	Power	kW	2.51	4.05	4.05
17	Power consumption	MWh/year	4.05	6.48	6.48
	Fans and pumps				
18	Power	kW	37.63	7.05	7.05
19	Power consumption	MWh/year	179.70	24.23	24.23
20	Comparison	%	100%	14.58%	14.58%
	Fan-Coils Dehumidifiers				
21	Power	kW		18.66	18.66
22	Power Consumption	MWh/year		43.09	43.09
	Cooling system				
23	Emission power	W/m^2	85	74	74
24	Power	kW	113.36	85.13	85.13
25	Summer power consumption	MWh/year	116.49	50.16	50.16
	Heating system				
26	Power	kW	91.83	87.75	87.75
27	Winter power consumption	MWh/year	80.99	30.91	30.91
28	Solar energy supply	MWh/year			- 74.08
	Circulators of water to the system				
29	Power	kW			0.95
30	Power consumption	MWh/year			3.22
31	Annual power consumption	MWh/year	197.48	148.29	77.43
	Comparison	**%**	**100%**	**75.09%**	**39.21%**

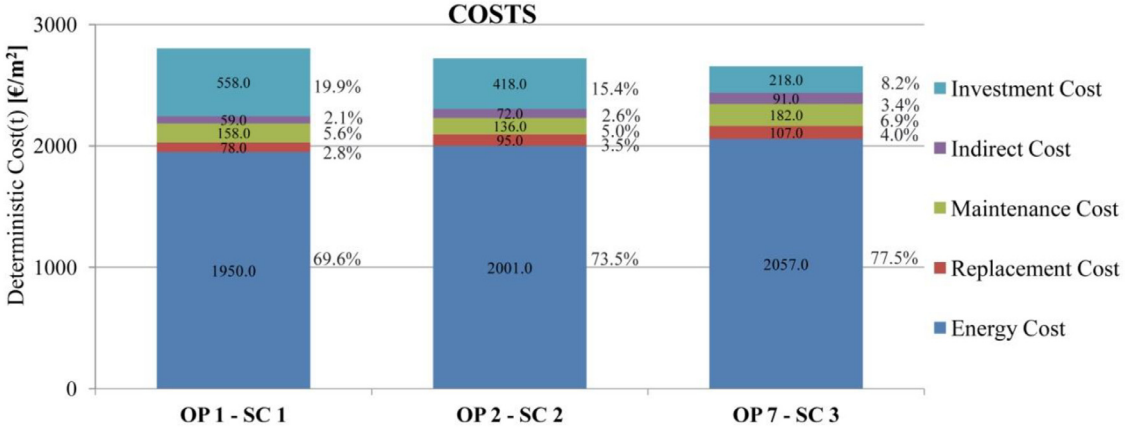

Fig. 18. Results of the Global Cost over 30 years applied to the 3 scenarios under study.

Valf Residual value (€)
R_R Real interest rate
Ri Inflation rate
Rint Interest rate
L Years of building service life
C_M Maintenance costs

Fig. 18 shows the results obtained. The estimation of the investment amortisation approach was based on experiences reported in other studies [33,84], and it could serve as a reference for other cultural buildings or administrative offices in Eastern Spain. To calculate the installation costs, we used databases of companies in the sector. The cost of installing 230 m^2 of solar thermal panels was based on a ratio of € 397/m^2, including labour costs, accumulation deposits or inertia, distribution equipment, circulation pumps, system management teams, and annual maintenance costs. A total cost of €91,450 was considered. Given that the investment in the installation system of 1417.5 m^2 of KaRo frames, including the

Table 9
Investment amortisation period of OP 2 and OP 7 compared to OP 1.

		OP 1	OP 2	OP 7	OP2-OP7
All-water installation with heat pump	€	119,070 €			
Installation with KaRo mats with TCP panels	€		202,869 €	294,319 €	
Annual energy consumption	kWh/yr	185,451.50	139,274.08	72,715.46	
Annual savings	€		6557.12	16,008.51	9451.32
Amortisation Period	**years**		**12.78**	**17.76**	**9.67**

cost of the two substations, floor distribution tubes in embedded pipes 32 mm in diameter and PPR circuits of 20 mm diameter pipes was 70.37% higher, we can approximate the amortisation period for that investment as expressed in Table 9.

The same could be done for the solar panel installation and the solar cold production system with lithium chloride LiCl, which account for a 45.5% increase in the cost of the capillary tube frames. To calculate the amortisation periods, a cost of 0.142 €/kWh [76] was taken into account. As shown, in the case of TCP panels, the investments could be amortised in the medium term, over 12 to 13 years (Table 9). In the case of thermal solar panels, the investment would be amortised in the long term compared to the all-air system or SC 1, that is, in 17.78 years. Compared to investments in radiant floor capillary tube mat TCP panels, the investment would be amortised over approximately 10 years. The decision to possibly implement these systems should take into account the high levels of comfort provided in homes and the significant drops in CO_2 emissions given the annual energy demand reductions of 31.47% (SC 2) or 77.48% (SC 3). These CO_2 emission reductions could be encouraged by public administrations, thus reducing users' installation costs, with shorter investment amortisation periods of around 8 to 10 years.

6. Conclusions

Radiant surface conditioning systems based on PPR capillary tube mats lead to high standards of comfort and significant energy savings. They are therefore healthier and environmentally friendly. They also allow using alternative energies such as solar energy. When the technology is implemented in coastal climates, with high values of outdoor air relative humidity in summer, dehumidification systems require finely tuned controls. It was possible to experiment and evaluate the system's behaviour using simulation tools at the Museum of the University of Alicante, on the Mediterranean coast. Three scenarios were examined. The first was the existing all-air conditioning system (SC 1). The second consisted in applying radiant floor TCP thermal ceramic panels (SC 2). The third was a variant of SC 2, incorporating renewable energy to the system via the installation of rooftop solar thermal panels (SC 3). To perform the comparison, users' experienced comfort parameters were adjusted in all three scenarios: mainly the operating temperature T_o, as well as sensible and latent heat transferred by the user. The following results were obtained:

- TCP panel systems are more energy efficient and more comfortable than the SC 1 system. Annual energy demand was 24.91% lower in SC 2 and 60.79% lower in SC 3.
- The investment increase due to the TCP panel capillary tube mat system could be amortised over a reasonable period of time, compared to a heat pump-based all-air system, with climate control and duct distribution (SC 1). In the case of the MUA under study, the €83,799 surcharge would be amortised in 12.78 years, with a drop of energy demand of 46,177 kWh/yr, an annual saving of €6557.12, and a cost of €0.142/kWh in the electric mix.
- If the system included the installation of 230 m^2 of rooftop solar thermal panels with water storage tanks and a triple phase absorption system through chemical energy accumulation with lithium chloride (LiCl), energy savings would be considerable. It would save 60.79% in the case of SC 1, and 47.79% in the case of SC 2. The investment in installation costs could be amortised in little under 18 years, with a yearly reduction of 12,469 kg of CO_2, and in 9.67 years compared to SC 2.

This research has shown that it is viable to implement radiant surface conditioning systems in public cultural buildings. They confer far greater comfort levels to users compared to convective systems. Investment return periods are between 12 and 18 years, provided a solar energy support system is used in latitudes with significant levels of annual solar radiation. These amortisation periods could be considerably reduced by implementing state subsidies. Such policies would be easy to justify due to the benefits derived from major drops in CO_2 emissions, the improvements to environmental management and a healthier environment.

In future studies, we will examine the energy consumption of TCP panels installed in two offices at the University of Alicante. Home automation monitoring of energy consumptions by means of electric metres and flowmetres will enable knowing the real levels of energy consumption due to dehumidification, and to quantify TCP panel energy saving more accurately.

Funding

This research has been funded by the projects "Generation of knowledge on the multisensory interaction of human beings with the environments for the development of new products and services in the ceramics sector (4SENSES)" (ACOMP/2010/040). Complementary aid for $R+D+i$ projects. Generalitat Valenciana. Ministry of Education. Spain, 2010; and "Research on sustainable architectural and bioclimatic conditioning solutions using ceramic materials (ASCER1-17I)". Spanish Association of Manufacturers of Ceramic Tiles and Flooring (ASCER). 2015–2017.

The funders had no role in the design of the study; in the collection, analyses, or interpretation of data; in the writing of the manuscript, or in the decision to publish the results.

Declaration of Competing Interest

The author declares no conflict of interest.

Acknowledgements

Our thanks to José Luis Sanjuan for his help in modelling the building with Design Builder; to Ginés Gómez Castelló for his helping in the monitorization of the MUA; and Carlos Rizo for his help in data collecting.

References

[1] C. Karmann, S. Schiavon, F. Bauman, Thermal comfort in buildings using radiant vs. all-air systems: a critical literature review, Build. Environ. 111 (2017) 123–131.
[2] T. Catalina, J. Virgone, F. Kuznik, Evaluation of thermal comfort usingcombined CFD and experimentation study in a test room equipped with acooling ceiling, Build. Environ. 44 (8) (2009) 1740–1750.

[3] Y. He, N. Li, M. He, D. He, Using radiant cooling desk for maintaining comfort in hot, Energy Build 145 (2017) 144–154.
[4] P. Mustakallio, Z. Bolashikov, L. Rezgals, A. Lipczynska, A. Melikov, R. Kosonen, Thermal environment in a simulated double office room with convective and radiant cooling systems, Build. Environ. 123 (2017) 88–100.
[5] K. Zhao, X.H. Liu, Y. Jiang, Application of radiant floor cooling in a large openspace building with high-intensity solar radiation, Energy Build. 66 (2013) 246–257.
[6] G.B. Zhou, J. He, Thermal performance of a radiant floor heating system with different heat storage materials and heating pipes, Appl. Energy 138 (2015) 648–660.
[7] Movinord Climatización S.L., Manual de Climatización Tranquila. Available online: http://www.movinord.com/descargas/Climatizacion%202008.pdf. (accessed on 11 March 2019).
[8] T. Mikeska, S. Svendsen, Dynamic behavior of radiant cooling system based on capillary tubesin walls made of high performance concrete, Energy Build 108 (2015) 92–100.
[9] R.J. de Dear, et al., Progress in thermal comfort research over the last twenty years, Indoor Air 23 (2013) 442–461.
[10] Beka, Capillary Tube Systems. Product Data Sheets, Beka Heiz-und Külmatten, Berlín, Germany, 2008. Technical Information G0 https://www.beka-klima.de/en/heating-cooling/capillary-tube-technology/. (accessed on 5 March 2019).
[11] V. Echarri Iribarren, A. Espinosa Fernández, A. Galiano Garrigós, Energy efficiency on flooded roofs: the University of Alicante Museum, WIT Trans. Eng. Sci. 106 (2016) 163–176.
[12] Climate Well TM10. Design Guidelines. Available online: http://www.solarcombiplus.eu/docs/SolarCombi_ClimateWell_trainingmaterial5.pdf. (accessed on 12 March 2019).
[13] C. Monné, S. Alonso, F. Palacín, Evaluación de una instalación de refrigeración por absorción con energía solar, Información Tecnológica 22 (2011) 39–41.
[14] M. Zamora, Empleo de bombas de calor acopladas a intercambiadores geotérmicos: Proyecto Geocool, Montajes e instalaciones: Revista técnica sobre la construcción e ingeniería de las instalaciones 38 (426) (2008) 66–72.
[15] S. Haiwen, D. Lin, L. Xiangli, Quasi-dynamic energy-saving judgment of electric-driven seawater source heat pump district heating system over boiler house district heating system, Energy Build 42 (2010) 2424–2430.
[16] Z. Li, H. Songtao, Research on the heat pump system using seawater as heat source or sink, Build. Energy Environ. 25 (2006) 34–38. http://en.cnki.com.cn/Article_en/CJFDTOTAL-JZRK200603008.htm.
[17] T. Imanari, T. Omori, K. Bogaki, Thermal comfort and energy consumption ofthe radiant ceiling panel system: comparison with the conventional all-airsystem, Energy Build. 30 (2) (1999) 167–175.
[18] J. Miriel, L. Serres, A. Trombe, Radiant ceiling panel heating-cooling systems: experimental and simulated study of the performances, thermal comfort andenergy consumptions, Appl. Therm. Eng. 22 (16) (2002) 1861–1873.
[19] L. Zhang, X.H. Liu, Y. Jiang, Experimental evaluation of a suspended metal ceiling radiant panel with inclined fins, Energy Build 62 (2013) 522–529.
[20] A. Koca, Z. Gemici, Y. Topacoglu, et al., Experimental investigation of heattransfer coefficients between hydronic radiant heated wall and room, Energy Build. 82 (2014) 211–221.
[21] S.S. Mi, K.N. Rhee, S.R. Ryu, et al., Design of radiant floor heating panel in viewof floor surface temperatures, Build. Environ. 92 (2015) 559–577.
[22] Y.T. Chae, R.K. Strand, Thermal performance evaluation of hybrid heat source radiant system using a concentrate tube heat exchanger, Energy Build. 70 (1) (2014) 246–257.
[23] B. Ning, Y. Chen, H. Liu, S. Zhang, Cooling capacity improvement for a radiant ceiling panel with uniform surface temperature distribution, Build. Environ. 102 (2016) 64–72.
[24] G. Lv, C. Shen, Z. Han, W. Liao, D. Chen, Experimental investigation on the cooling performance of a novel grooved radiant panel filled with heat transfer liquid, Sustain. Cities Soc. (2019). https://doi.org/10.1016/j.scs.2019.101638.
[25] V. Cantabella, et al., Dinamycs of the thermal performance of an electric radiant floor with removable ceramic tiles, in Proc. of XI Congreso Mundial de la Calidad del Azulejo y del Pavimento QUALICER 10, Castellón, 15th February 2010. http://www.qualicer.org/recopilatorio/ponencias/ponencias.php?valor=&autorvalor=&tipovalor=0&tipo=1&ano=2010&tipoano=1&enviado=&idioma=en.
[26] V. Echarri Iribarren, A.L. Galiano Garrigós, A.B. González Avilés, Ceramics and healthy heating and cooling systems: thermal ceramic panels in buildings. Conditions of comfort and energy demand versus convective systems, Informes de la Construcción 68 (2016) 19–32. http://informesdelaconstruccion.revistas.csic.es/index.php/informesdelaconstruccion/article/view/5803/6693.
[27] M. Kottek, J. Grieser, C. Beck, B. Rudolf, F. Rubel, World map of the Köppen-Geiger climate classification updated, Meteorol. Z. 15 (3) (2006) 259–263.
[28] M. Kottek, J. Grieser, C. Beck, B. Rudolf, F. Rubel (2006), F. Rubel, K. Brugger, K. Haslinger, I. Auer (2017), World map of the Köppen-Geiger climate classification updated. High resolution map and data (version March 2017). KMZ file for Google Earth (high res): gGlobal_1986-2010_KG_5 m.kmz, Climate Change & Infectious Diseases, Meteorologische Zeitschrift 26 (2) (2017) 115-125. http://koeppen-geiger.vu-wien.ac.at, Wien, Published Mar 2017. (accessed on 13 April 2019).
[29] Ministerio de Vivienda, Real Decreto 314/2006 de 17 de marzo. Código Técnico de la Edificación, CTE. Boletín Oficial del Estado, n° 74, 28 de marzo de 2006, pp. 11816-11831. Available online: http://www.codigotecnico.org/images/stories/pdf/realDecreto/RD3142006.pdf. (accessed on 16 April 2019).
[30] V. Echarri, A.B. González, M.I. Pérez, Refreshing architectural spaces by means of large-sized vertical ceramic panels, in Proc. of XII Congreso Mundial de la Calidad del Azulejo y del Pavimento QUALICER 12, Castellón, 13th February 2012. http://www.qualicer.org/recopilatorio/ponencias/ponencias.php?valor=&titulo=1&autorvalor=Echarri&tipovalor=0&tipo=1&ano=2012&tipoano=1&enviado=&idioma=en.
[31] V. Echarri, E. Oviedo, V. Lázaro, Panel de Acondicionamiento Térmico Cerámico. Patent P201001626, 28. INVENES, OEPM – Oficina Española de Patentes y Marcas (2010). http://invenes.oepm.es/InvenesWeb/detalle?referencia=P201001626. (Accesed on 10 March 2019).
[32] C. Zanelli, et al., Porcelain stonware large slabs processing and technological properties, in Proc. of XI Congreso Mundial de la Calidad del Azulejo y del Pavimento QUALICER 10, Castellón, 15th February 2010. http://www.qualicer.org/recopilatorio/ponencias/ponencias.php?valor=&titulo=1&autorvalor=Zanelli&tipovalor=0&tipo=1&ano=2010&tipoano=1&enviado=&idioma=en.
[33] V. Echarri-Iribarren, C. Rizo-Maestre, F. Echarri-Iribarren, Healthy climate and energy Savings: using thermal ceramic panels and solar thermal panels in Mediterranean housing blocks, Energies 11 (2018) 2707, doi:10.3390/en11102707.
[34] E.Xaar Knight, Innovative inkjet technology for the ceramic tile industry, in: Digital Decoration of Ceramic Tiles, Modena, Italy, ACIMAC, 2009, pp. 70–73.
[35] I. Hutchings, Ink-jet printing for the decoration of ceramic tiles: technology and opportunities, in: Proc. of XI Congreso Mundial de la Calidad del Azulejo y del Pavimento QUALICER 10, Castellón, 2010, 15, febrero 15th February 2010.
[36] C. Peng, Z. Wu, Measuring and analyzing frequency responses of heat conduction in Nanjing buildings under in situ conditions, Indoor Built Environ. 18 (4) (2009) 285–292, doi:10.1177/1420326x09104139.
[37] V. Echarri, A.L. Galiano, M.I. Pérez, A.B. González, Conditioning systems by radiant surfaces: comparative analysis of thermal ceramic panels versus the conventional systems in a museum, WIT Trans. Eng. Sci. 83 (2014) 1–12.
[38] T. Theodosiou, K. Tsikaloudaki, K. Kontoleon, D. Bikas, Thermal bridging analysis on cladding systems for building facades, Energy Build 109 (2015) 377–384. https://doi.org/10.1016/J.ENBUILD.2015.10.037.
[39] EN ISO 7730:2005, Ergonomics of the Thermal Environment: Analytical Determination and Interpretation of Thermal Comfort Using Calculation of the PMV and PPD Indices and Local Thermal Comfort Criteria, International Organization for Standardization, Geneva, 2005. https://standards.cen.eu/dyn/www/f?p=204:110:0::::FSP_PROJECT,FSP_ORG_ID:3603,6104&cs=174E4319C250BD68D73B1BF5E1B13A151. (accesed on 10 June 2019).
[40] O.P. Fanger, Thermal Comfort Analysis and Applications in Environmental Engineering, McGraw-Hill Book Company, New York, 1970.
[41] American Society of Heating, Refrigeration and Air Conditioning Engineers. Handbook of Fundamentals, ASHRAE, Atlanta, GA, USA, 2017. Available online: https://www.ashrae.org/technicalresources/ashrae-handbook/description-2017-ashrae-handbook-fundamentals. (Accesed on 20 March 2019).
[42] J.M. Sala Lizarraga, et al., Transmisión de calor en edificios, in: R. Hernández, et al. (Eds.), Arquitectura Ecoeficiente, I, Eds., Servicio Editorial de la UPV/EHU, San Sebastián, 2012, pp. 33–62. https://www.academia.edu/32701021/Arquitectura_Ecoeficiente._Tomo_I. Chapter 2.
[43] A. Monge-Barrio, A. Sánchez-Ostiz, Energy efficiency and thermal behaviour of attached sunspaces in the residential architecture in Spain. Summer conditions, Energy Build. 108 (2015) 244–256.
[44] Ministerio de Fomento, Orden FOM/1635/2013, de 10 de septiembre, por la que se actualiza el Documento Básico DB-HE «Ahorro de Energía», del Código Técnico de la Edificación, Boletín Oficial del Estado, n° 219, 10 de septiembre de (2010) 67137–67209. Available online: https://www.codigotecnico.org/images/stories/pdf/ahorroEnergia/DBHE.pdf. (Accesed on 20 March 2019).
[45] Y. Liu, J. Zhang, Model study of the influence of ambient temperature and installation types on surface temperature measurement by using a fiber bragg grating sensor, Sensors 16 (7) (2016) 975, doi:10.3390/s16070975.
[46] V. Echarri, A. Espinosa, C. Rizo, Thermal transmission through existing building enclosures: destructive monitoring in intermediate layers versus non-destructive monitoring with sensors on surfaces, Sensors 17 (2017) 2848.
[47] J. Feijó-Muñoz, C. Pardal, V. Echarri, J. Fernández-Agüera, R. Assiego de Larriva, M. Montesdeoca Calderín, I. Poza-Casado, M.A. Padilla-Marcos, A. Meiss, Energy impact of the air infiltration in residential buildings in the Mediterranean area of Spain and the Canary islands, Energy Build. 188–189 (2019) 226–238.
[48] UNE-EN ISO 52016-1:2017. Energy performance of buildings - Energy needs for heating and cooling, internal temperatures and sensible and latent heat loads - Part 1: Calculation procedures (ISO 52016-1:2017). Madrid, Spain, 2017. Available online: https://www.aenor.com/normas-y-libros/buscador-de-normas/une/?Tipo=N&c=N0059143. (accesed on 12 March 2019).
[49] R. Albatici, A.M. Tonelli, M.A. Chiogna, A comprehensive experimental approach for the validation of quantitative infrared thermography in the evaluation of building thermal transmittance, Appl Energy 141 (2015) 218–228.
[50] V. Echarri, M. Salvador, G. Ramírez, A. Espinosa, Lesiones en paneles fenólicos de madera baquelizada: diagnóstico e intervención, in: Proccedings of 4th Congreso de Patología y Rehabilitación de Edificios (PATORREB)., Santiago de Compostela, Spain, 15 February 2012, p. 206.
[51] G. Ficco, F. Iannetta, E. Ianniello, F. Romana, A. d'Ambrosio, M. Dell'Isola, U–value in situ measurement for energy diagnosis of existing buildings, Energy Build. 104 (2015) 108–121.

[52] J.A. Márquez, M.M. Bohórquez, S.G. Melgar, A new metre for cheap, quick, reliable and simple thermal transmittance (U-Value) measurements in buildings, Sensors 17 (2017) 2017.
[53] T. Theodosioua, K. Tsikaloudakia, D. Bikasa, Analysis of the thermal bridging effect on ventilated facades, Procedia Environ. Sci. 38 (2017) 397–404.
[54] A. Ghaffarianhoseini, T. Zhang, O. Nwadigo, A. Ghaffarianhoseini, N. Naismith, J. Tookey, K. Raahemifar, Application of nD BIM integrated knowledge-based building management system (BIM-IKBMS) for inspecting post-construction energy efficiency, Renew. Sustain. Energy Rev. 72 (2017) 935–949.
[55] Directive 2010/31/EU of the European Parliament and of the Council of 19 May 2010 on the energy performance of buildings - EPBD. Strasbourg, France, 2010. Available online: https://eurlex.europa.eu/legal-content/EN/ALL/?uri=CELEX%3A32010L0031. (Accesed on 15 March 2019).
[56] HULC. Herramienta unificada Lider-Calener. Orden FOM/1635/2013, de 10 de septiembre (BOE de 12 de septiembre), por la que se actualiza el Documento Básico DB HE "Ahorro de Energía", del CTE. Available online: https://www.codigotecnico.org/index.php/menu-recursos/menu-aplicaciones/282-herramientaunificada-lider-calener.html. (accessed on 9 March 2019).
[57] Z. Rahimpoura, A. Faccani, D. Azuatalam, A. Chapman, G. Verbič, Using thermal inertia of buildings with phase change material for demand response, Energy Procedia 121 (2017) 102–109.
[58] European Commission. Action Plan for Energy Efficiency: Realising the Potential; Commission StaffWorking Document, 545 Final. 2006. Available online: http://ec.europa.eu/transparency/regdoc/rep/1/2006/ES/1-2006-545-ES-F1-1.Pdf- (accessed on 16 May 2019).
[59] K. Bataineh, Y. Taamneh, Review and recent improvements of solar sorption cooling systems, Energy Build. 128 (2016) 22–37.
[60] I. Sarbu, C. Sebarchievici, Review of solar refrigeration and cooling systems, Energy Build. 67 (2013) 286–297.
[61] M. Balghouthi, M.H. Chahbani, A. Guisan, Investigation of a solar cooling installation in Tunisia, Appl Energy 98 (2012) 138–148.
[62] E. Marrasso, C. Roselli, M. Sasso, F. Tariello, Analysis of a hybrid solar-assisted trigeneration system, Energies 9 (2016) 705.
[63] K. Gaspar, M. Casals, M. Gangolells, A comparison of standardized calculation methods for in situ measurements of façades U-value, Energy Build. 130 (2016) 592–599.
[64] ISO 9869-1:2014, Thermal Insulation. Building Elements. In-Situ Measurement of Thermal Resistance and Thermal Transmittance. Part 1: Heat Flow Metre Method, International Organization for Standardization, Geneva, Switzerland, 2014. Available online: https://www.iso.org/standard/59697.html. (accessed on 15 March 2019).
[65] L. Evangelisti, C. Guattari, P. Gori, R. Vollaro, In situ thermal transmittance measurements for investigating differences between wall models and actual building performance, Sustainability 7 (, 8) (2015) 10388–10398.
[66] D. Bienvenido-Huertas, J. Moyano, D. Marin, R. Fresco-Contreras, Review of in situ methods for assessing the thermal transmittance of walls, Renew. Sustain. Energy Rev. 102 (2019) 356–371.
[67] A.H. Deconinck, S. Roels, Comparison of characterisation methods determining the thermal resistance of building components from onsite measurements, Energy Build. 130 (2016) 309–320.
[68] V. Echarri, Thermal ceramic panels and passive systems in Mediterranean Housing: energy savings and environmental impacts, Sustainability 9 (2017) 1613.
[69] R.W. Mossa, P. Henshall, F. Arya, G.S.F. Shire, T. Hyde, P.C. Eames, Performance and operational effectiveness of evacuated flat plate solar collectors compared with conventional thermal, PVT and PV panels, Appl Energy 216 (2018) 588–601.
[70] Ch. Lamnatou, G. Notton, D. Chemisana, C. Cristofari, The environmental performance of a building-integrated solar thermal collector, based on multiple approaches and life-cycle impact assessment methodologies, Build. Environ. 87 (2015) 45–58.
[71] S.P. Kavanaugh, K. RaffertyGround-source Heat Pumps, Design of Geothermal System For Commercial and Institutional Buildings, ASHRAE Applications Handbook, Atlanta, GA, US, 1997.
[72] S. Rosiek, F.J. Batlles, Shallow geothermal energy applied to a solar-assisted air-conditioning system in southern Spain: two-year experience, Appl Energy 100 (2012) 267–276.
[73] C.R. Ruivo, P.M. Ferreira, D.C. Vaz, On the error of calculation of heat gains through walls by methods using constant decrement factor and time lag values, Energy Build. 60 (2013) 252–261.
[74] C. Stetiu, Energy and peak power savings potential of radiant cooling systems in US commercial buildings, Energy Build 30 (1999) 127–138. https://doi.org/10.1016/S0378-7788(98)00080-2.
[75] European Comission. LCDN - The Life Cycle Data Network. Available online: https://eplca.jrc.ec.europa.eu/LCDN/. (accessed on 9 March 2019).
[76] IDAE. Informe de Precios Energéticos Regulados. Julio 2017. http://www.idae.es/sites/default/files/estudios_informes_y_estadisticas/tarifas_reguladas_julio_2017.pdf. (accessed on 7 March 2019).
[77] B. Choudhury, B.B. Saha, P.K. Chatterjee, J.P. Sarkar, An overview of developments in adsorption refrigeration systems towards a sustainable way of cooling, Appl Energy 104 (2013) 554–567.
[78] J.M. Sancho Ávila, J. Riesco Martín, C. Jiménez Alonso, M.D. Sánchez de Cos, J. Montero Cadalso, M. López Bartolomé, Atlas de radiación solar en españa utilizando datos del SAF de Clima de EUMETSAT, Madrid. (2005). Available online: https://www.aemet.es/documentos/es/serviciosclimaticos/datosclimatologicos/atlas_radiacion_solar/atlas_de_radiacion_24042012.pdf. (accessed on 10 March 2019).
[79] R. Aroca-Delgado, J. Pérez-Alonso, A.J. Callejón-Ferre, B. Velázquez-Martí, Compatibility between crops and solar panels: an overview from shading systems, Sustainability 10 (2018) 743.
[80] R. Valančius, A. Jurelionis, R. Jonynas, V. Katinas, E. Perednis, Analysis of medium-scale solar thermal systems and their potential in Lithuania, Energies 8 (2015) 5725–5737.
[81] C. Prieto, A. Rodríguez, D. Patiño, L.F. Cabeza, Thermal energy storage evaluation in direct steam generation solar plants, Solar Energy 159 (2018) 501–509.
[82] B. Corona, C. de la Rúa, G. San Miguel, Socio-economic and environmental effects of concentrated solar power in Spain: a multiregional input output analysis, Solar Energy Mater. Solar Cell. 156 (2016) 112–121.
[83] UNE-EN 15459-1:2017. Energy performance of buildings - Economic evaluation procedure for energy systems in buildings - Part 1: Calculation procedures, Module M1-14. CEN. European Committee for Standardization, Brussels, Belgium, 2017. Available online: https://standards.cen.eu/dyn/www/f?p=204:110:0::::FSP_PROJECT,FSP_ORG_ID:40932,6209&cs=110690DD8F9BE238B61D722D035C11CAE. (accesed on 11 June 2019).
[84] E. Di Giuseppe, M. Iannaccone, M. Telloni, M. D'Orazio, C. Di Perna, Probabilistic life cycle costing of existing buildings retrofitinterventions towards nZE target: methodology and applicationexample, Energy Build. 144 (2017) 416–432.